

CATALYST Cue

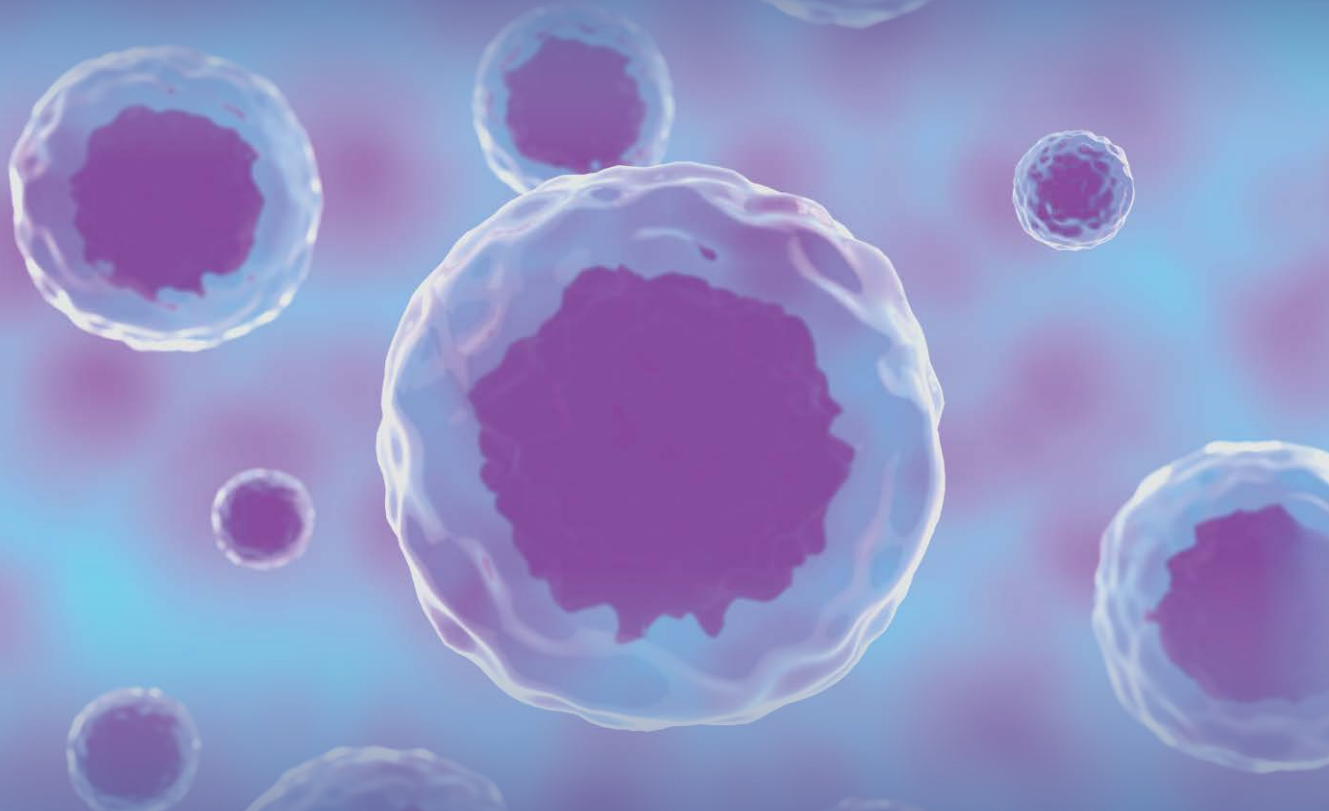
VOLUME 01

ISSUE 06

JUNE 2025

TRANSFORMATIVE TOOLS AIDING BIOTHERAPIES

MASTER PRECISION FREEZE DRYING FOR LONG-TERM STORAGE USING
THE  LYOVAPOR™ L-250 PRO



DISCOVER DEEPER INSIGHTS
PHOTON ETC LIGHTIR™

IN VIVO FLUORESCENCE IMAGING FOR NIR-I &
NIR-II RESEARCH IN SMALL AND LARGE ANIMALS

3-COLOR WESTERN BLOT
MADE SIMPLE

A PRACTICAL GUIDE

18th - 20th September 2025, Hitex Hyd
Booth No: C21, Hall No: 03

 analytica Lab India



39+ Years of Pioneering the Scientific Frontier

Inkarp, established in 1985, honors 39 years of dedication to the scientific community in India. Our journey continues to be driven by the pursuit of excellence in **offering cutting-edge scientific research instruments**. We take pride in providing scientists across the country with tools that facilitate discoveries and innovation.



Scan
to view our website

Follow Us On



From the editor



Dear Readers,

It gives me great pride to present the sixth issue of CATALYSTCue. With this, we complete the first volume of our magazine — a journey that began with the goal of making research insights and applications more accessible to scientists everywhere.

The cover story of this issue focuses on the growing impact of single-cell omics. Understanding biology at the level of individual cells is unlocking new possibilities in healthcare, life sciences, and biotechnology.

In the features section, we dive into two important areas — how post-translational modifications influence biological systems, and a retrospective view on protein-small molecule interactions and their role in modern research.

The applications section brings together real-world methods across different areas of laboratory science.

You will find practical studies on:

- Measuring bacterial growth and protein content with improved workflows.
- Precision freeze drying of yeast-loaded microcapsules for long-term storage.
- Detecting adulterants in morphine sulphate solutions with high sensitivity.
- Live cell imaging and manipulation using bio-AFM technologies.
- Advancements in preclinical imaging and radiation therapy systems.
- Studying binding affinity and residence time for antiretroviral compounds.
- Quantifying monoclonal antibody light chains with triple quadrupole mass spectrometry.
- Using structured illumination for deeper, more precise fluorescence imaging.

Our Tech Corner explains in simple steps how to develop a 3-color western blot — a powerful tool for protein research that can strengthen your lab's capabilities.

The Product Highlight showcases flexible imaging solutions for live, non-invasive research, offering better ways to study biological processes in real-time.

Throughout the past year, many of you have shared valuable feedback and suggestions. We want you to know that we have heard you, and we are continuously working to tailor CATALYSTCue to better meet the needs of the scientific community.

As we close Volume 1, we sincerely thank you for your support. We are excited to continue this journey with you.

Stay tuned — Volume 2 of CATALYSTCue will bring even more practical insights, research applications, and innovations designed to support your work.

Best regards,

Arun Mathrubootham
Director
Inkarp Instruments Pvt. Ltd.

Contents

Cover Story

- 01 The Single-Cell Omics Resolution

Features

- 04 Post-Translational Modification: Identification of Phosphorylation-Activated States in Proteins
- 09 Protein-Small Molecule Biomolecular Interactions – a Retrospective

Interview

- 16 Inside BioArtha Labs: Leadership, Science, and the Business of Innovation

Mr. Ganesh

co-founder, BioArtha Labs

Application Showcase

- 19 Freeze drying of beads containing yeasts in the BUCHI Lyovapor™ L-200 Pro
- 24 High-speed *in vivo* imaging using the Lambert HiCAM Fluo
- 27 Using Reichert Surface Plasmon Resonance (SPR) for Screening of Small Molecule Inhibitors
- 30 A Robust LC-MS/MS Method for the Quantification of Monoclonal Antibody Utilizing the Waters Xevo TQ-XS Mass Spectrometer
- 38 Optical Sectioning in Widefield Fluorescence Microscopy with ZEISS Apotome

Contents

- 46** Live Cell Imaging and Manipulation with Nanosurf Bio-AFM
- 51** Preclinical Imaging and Radiation Therapy with Precision X-Ray SmART+ and X-Rad Systems
- 54** Detection of Adulterants in Morphine Sulphate Solutions using the Implen UV/Vis NanoPhotometer®

Tech Corner

- 57** Developing a 3-Color Western Blot: What You Need to Know to Get Started

Product Highlight

- 63** Advancing in vivo Fluorescence Imaging: LIGHTIR™ for NIR-I/NIR-II Research in Small and Large Animals

Industry Buzz

- 65** Rx updates: Recent novel FDA approved drugs
- 66** A sneak-peak at our events

Editor

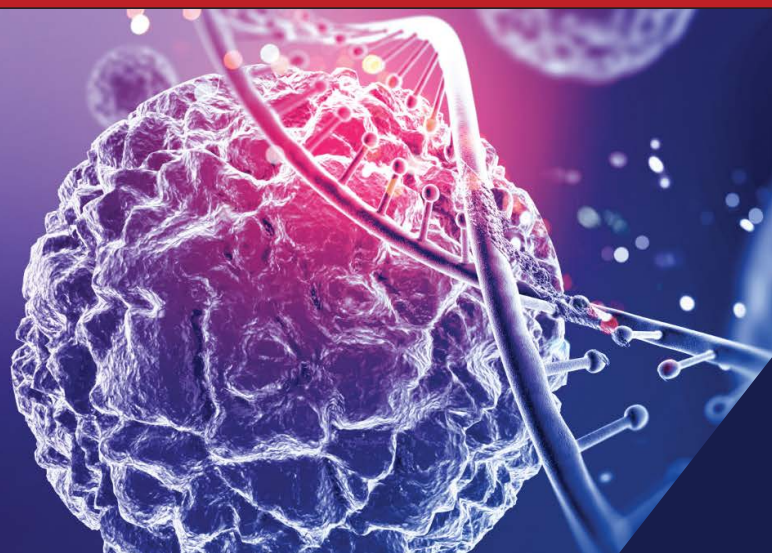
Arun Mathrubootham

Creative Team

Apoorva Nagarajan
Halim Baig
Dasari Raju

Marketing Team

Venkata Pavan Kumar
Sanghavi Suresh



The Single-Cell Omics Resolution

Over the past 20 years, developments in molecular biology have fundamentally changed how we think about health and illness. The advent of single-cell omics, a collection of technologies that permits molecular study at the level of individual cells, is one of the most groundbreaking advancements. Single-cell omics enables the accurate dissection of cellular diversity, heterogeneity, and dynamic states, in contrast to conventional bulk sequencing techniques that average signals across heterogeneous populations.

With previously unheard-of granularity, researchers can now identify rare cell types, track developmental trajectories, uncover pathogenic mechanisms, and characterise responses to therapeutic interventions by enabling high-throughput analysis of genomes, transcriptomes, epigenomes, proteomes, and metabolomes at single-cell resolution. These developments are becoming more and more important in the fields of developmental biology, cancer immunotherapy, precision medicine, and ageing studies.

The Argument in Favour of Single-Cell Settlement

Because conventional approaches average chemical signals from millions of cells, they frequently mask important discoveries. On the other hand, single-cell technologies enable researchers to fully capture the range of biological variability by revealing each cell's unique molecular identity and functional state. In complicated tissues like tumours, where uncommon subpopulations may contribute to therapy resistance, or in the ageing brain, where minute transcriptional changes in glial cells can impact the course of disease, this ability is particularly crucial.

Important Platforms for Technology

Single-cell omics encompasses a variety of methods:

- Transcriptomic patterns are captured using single-cell RNA sequencing (scRNA-seq), which is used to categorise different cell types and states.
- Somatic mutations, copy number variations, and genomic instability are detected by single-cell DNA sequencing.

Epigenomics with single-cell ATAC-seq:

- Uncovering regulatory landscapes and chromatin accessibility.
- Proteins and post-translational changes are quantified using single-cell proteomics.

Measuring cellular metabolism and metabolic alterations is known as single-cell metabolomics.

Multi-modal platforms that can analyse two or more omic layers within a single cell at the same time have been made possible by recent advancements. These platforms give a more comprehensive understanding of cell biology by shedding light on the interactions between transcriptome and protein abundance or between gene expression and epigenetic control.

Applications of Transformation in Various Fields

Single-cell omics is useful in many biological domains:

Oncology: Intratumoral heterogeneity and subclones linked to resistance and relapse have been revealed by scRNA-seq, which has completely changed the classification of tumours. It has also influenced the creation of therapeutic targets specific to cell types and the identification of biomarkers.

Neuroscience: Age-related changes in microglial states, neuronal diversity, and inflammatory markers linked to neurodegenerative illnesses including Alzheimer's and Parkinson's have been identified by single-cell transcriptome analysis of the brain.

Developmental Biology: Progenitor population identification and developmental lineage reconstruction are made possible by pseudo temporal ordering. This makes it easier to track organogenesis and find regulatory networks unique to a given lineage.

Regenerative Medicine: Targeted treatments, cellular reprogramming, and tissue engineering techniques are being developed with the use of insights into stem cell differentiation pathways. The ability to precisely manipulate regeneration potential at the cellular level is made possible by single-cell omics.

Immunology: The development of tailored immunotherapies and vaccines is aided by the characterisation of immune cell states during infection, inflammation, and autoimmune. It has been useful in monitoring immunological memory, cytokine patterns, and T cell exhaustion.

A worldwide reference framework is being established by large-scale projects like the Human Cell Atlas, Tabula Sapiens, and organ-specific atlases.

By cataloguing all human cell types and states across developmental stages and illness circumstances, these combined initiatives are anticipated to reshape our understanding of normal physiology and pathology.

Ethical Aspects

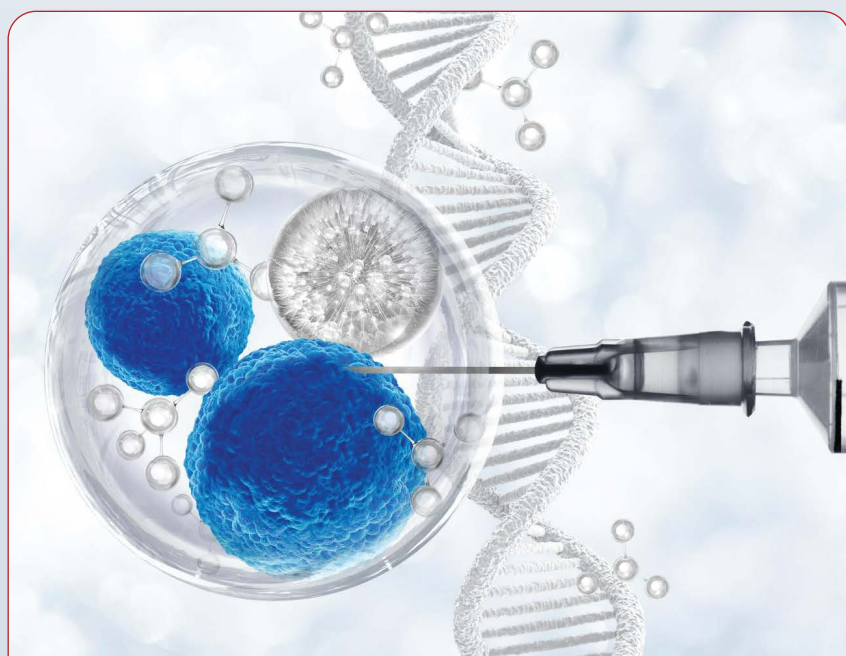
Single-cell omics presents both practical and ethical issues, as is the case with any potent technology. Concerns about data privacy, informed permission, and the possibility of predictive information misuse are raised by the ability to infer disease propensity from single-cell profiles. Establishing ethical standards for data sharing and use is likewise becoming more and more important, particularly in commercial and therapeutic settings.

Technical difficulties include computing complexity, data sparsity, batch effects, and bias in sample preparation. To guarantee repeatability, accuracy, and cross-study comparability, strong data integration frameworks, standardisation procedures, and scalable bioinformatics pipelines are necessary.

Prospects for the Future

Integration of single-cell omics with longitudinal research, artificial intelligence, and spatial biology is key to its future. These technologies are anticipated to speed up pattern detection, predictive modelling, and customised therapy design when combined with machine learning algorithms.

One paradigm change in biological research is single-cell omics. It is giving vital insights into the mechanisms behind development, ageing, illness, and health by making molecular analysis at the cellular level possible. The technique has the potential to enable genuinely personalised medicine, where treatments and diagnostics are based on each individual cell's distinct molecular fingerprint rather than averages, as it develops and is progressively incorporated into clinical procedures.



Post-Translational Modification

Identification of Phosphorylation-Activated States in Proteins

Identifying Akt/PKB and STAT3 phosphorylation states as prognostic factors in clear cell renal cell Carcinoma using QF-Pro®

Clear cell renal cell carcinoma (ccRCC) presents significant challenges in clinical management due to its resistance to conventional therapies and genetic heterogeneity. The QF-Pro® platform, based on an enhanced and simplified two-site Förster Resonance Energy Transfer (FRET) assay combined with Fluorescence Lifetime Imaging Microscopy (FLIM), enables precise quantification of post-translational modifications (PTMs).

The phosphorylation activation states of protein kinase B (PKB/Akt) and STAT3 were quantified to investigate their potential as prognostic biomarkers and their relevance to the development of personalized treatment strategies in patients with ccRCC.

1. Introduction

1.1. Background on ccRCC

Clear cell renal cell carcinoma is the most common and aggressive subtype of renal cell carcinoma. Due to its radioresistance, chemoresistance, and genetic

variability, ccRCC presents substantial therapeutic challenges. With 40% of patients experiencing mortality within five years post-diagnosis, there is an urgent need for reliable prognostic markers to guide personalised treatment.

Our research indicates that monitoring oncoprotein activation states—specifically PKB/Akt and STAT3—via QF-Pro® may provide a promising diagnostic tool with prognostic relevance.

1.2. Current limitations in ccRCC biomarker assessment

Traditional diagnostic methods largely rely on immunohistochemistry (IHC) to detect protein expression levels. While IHC provides a basic measurement, it does not reveal the activation state or the functionality of a protein, therefore missing relevant information about the biology of the disease. Conversely, QF-Pro® enables the quantitative evaluation of oncoprotein activation states by measuring the interactions between fluorophore-labelled antibodies targeting specific phosphorylation.

2. QF-Pro® technology and methodology

2.1. Principles of QF-Pro®

FRET is a non-radiative energy transfer technique that occurs between two fluorophores (donor and acceptor) when they are within 10 nanometres. FRET-FLIM provides additional precision by measuring changes in fluorescence lifetime, providing precise and quantitative values.

In this study, QF-Pro®, based on our proprietary two-site amplified FRET-FLIM method, was used to assess the activation states of PKB/Akt and STAT3 through phosphorylation-specific antibodies targeting key activation sites. The two-site assay achieves enhanced specificity due to the intrinsic spectroscopic properties of the FRET signal. The 1-10 nm working distance of QF-Pro®, coupled with the two-site labelling, eliminates false positive results.

2.2. Sample preparation and analysis

Formalin-fixed paraffin-embedded (FFPE) tissue microarrays (TMAs) from primary and metastatic ccRCC samples were analysed.

Each sample underwent QF-Pro® analysis using secondary QF-Pro® probes tagged with ATTO 488 (donor) and Alexa594 (acceptor) fluorophores. QF-Pro® activation state scores were then calculated for each patient.

3. Results

3.1. PKB/Akt activation upon EGF stimulation in cells

The activation dynamics of Akt/PKB (measured via phosphorylation at threonine-308) in cells were evaluated following stimulation with epidermal growth factor (EGF) using QFPro® technology (Figure 1A). QF-Pro® activation maps revealed significant differences in Akt activation between basal and EGF-stimulated conditions.

Under basal conditions (non-stimulated), the QF-Pro® maps showed cells predominantly in blue, indicative of minimal Akt phosphorylation. However, after 10 minutes of EGF stimulation, these maps shifted markedly, with cells exhibiting green to yellow signals. Orange pixels indicate areas of higher Akt/PKB activation state occurring at the plasma membrane of these cells (Figure 1B).

This transition reflects the phosphorylation and subsequent activation of Akt/PKB, detected via the QF-Pro® signal.

Quantitative analysis of phospho-Akt activation over time further confirmed these observations. Measurements taken at 1, 2, 5, and 10 minutes post-EGF stimulation demonstrated a significant progressive increase in Akt phosphorylation, with the highest activation observed at 10 minutes (Figure 1C). The high dynamic range and sensitivity of QF-Pro® allowed for precise visualisation and quantification of these activation states.

3.1. PKB/Akt activation in ccRCC progression

The activation state of Akt/PKB in ccRCC TMAs was evaluated across renal control tissues, primary tumours, and metastatic samples using the QF-Pro® assay. QF-Pro® maps demonstrated distinct differences in Akt/PKB activation among these groups. Primary tumour samples exhibited low activation levels, with QF-Pro® maps predominantly green. In contrast, metastatic tissues showed an increase in Akt/PKB activation, indicated by the transition to yellow and red pixels, reflecting higher phosphorylation levels (Figure 2A). Quantitative QF-Pro® scores confirmed these findings. Renal control tissues exhibited minimal Akt/PKB activation, while primary ccRCC tumour samples showed a mild increase. However, only metastatic samples showed a significantly higher activation state compared to both renal control tissue and primary tumours (Figure 2B). These results underscore the progressive activation of Akt/PKB during ccRCC progression and metastasis, suggesting its utility as a

Features

biomarker for disease aggressiveness and tumour evolution.

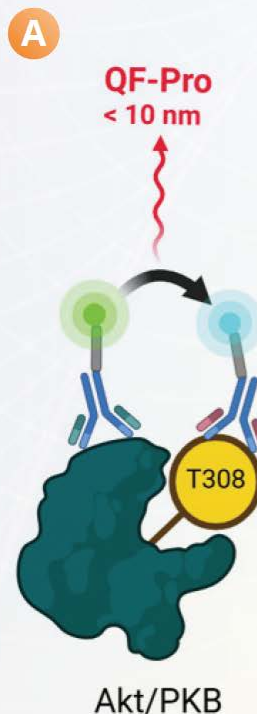


Figure 1A: Illustration of QF-Pro® assay for detecting Akt/PKB activation.

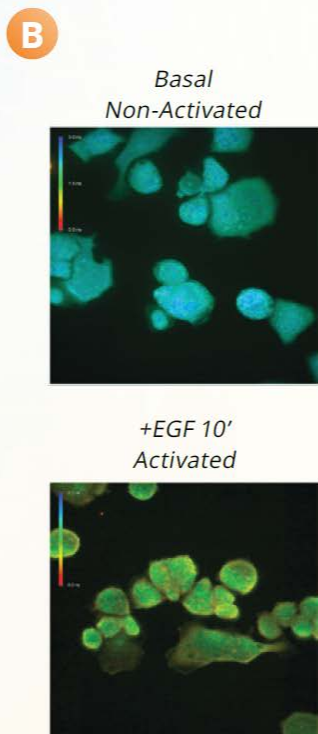


Figure 1B: Representative QF-Pro® maps show minimal Akt/PKB activation under basal conditions and increased phosphorylation upon EGF stimulation for 10 minutes.

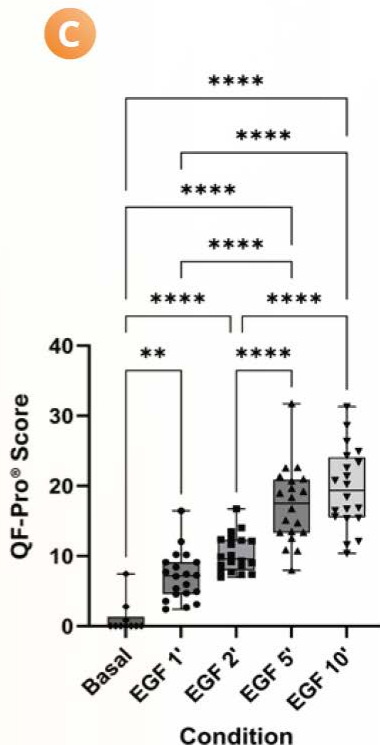


Figure 1C: Quantitative QF-Pro® scores across different EGF treatment time points demonstrate a significant increase in activation state with longer stimulation times ($p < 0.001$).

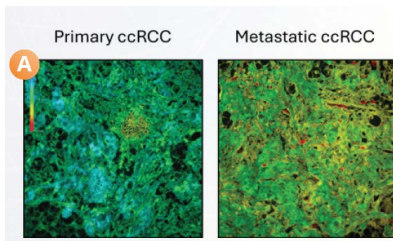


Figure 2A: Representative fluorescence lifetime images, primary ccRCC tissue shows moderate Akt/PKB activation (blue/green) and metastatic ccRCC tissue exhibits increased activation (yellow/red).

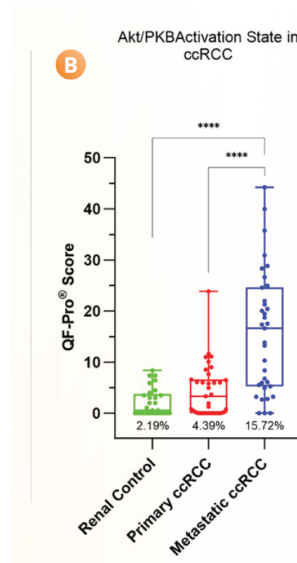


Figure 2B: QF-Pro® Score demonstrated a significant difference between non-cancerous, primary, and metastatic samples ($p < 0.001$), confirming that Akt activation state, rather than mere expression levels, correlates with clinical prognosis in ccRCC patients.

3.3. Prognostic precision of QF-Pro® versus IHC

QF-Pro® technology demonstrated superior prognostic precision compared to traditional IHC in detecting variations in Akt/PKB activation states across patient samples. This was evident from the survival analysis, where Kaplan-Meier survival curves based on QF-Pro scores provided a significantly stronger prognostic correlation compared to protein expression levels measured by IHC intensity.

In the QF-Pro® analysis, patients with higher Akt/PKB activation (upper quartile, red line) exhibited significantly poorer overall survival compared to those with lower activation levels (lower three quartiles, blue line) (Figure 3A). This finding indicates that increased Akt/PKB activation is associated with worse survival outcomes, underscoring its role as a marker of tumour aggressiveness and outcome.

Conversely, survival analysis based on the IHC intensity of pT308 Akt/PKB failed to show a significant association with survival, highlighting its lower prognostic value (Figure 3B). These differences can be attributed to the fundamental limitations of IHC, which measures only the expression level of a protein without providing insights into its activation state. Moreover, being a one-site assay, IHC is susceptible to the false positives that arise from the lack of specificity of primary antibodies.

These findings highlight the ability of QF-Pro® to assess activation states in FFPE tissues, accurately correlating high Akt/PKB activation with poorer survival, highlighting its value for understanding tumour behaviour and guiding clinical decisions in ccRCC.

3.4. STAT3 activation dynamics

Finally, the activation state of Tyr705-STAT3, a key phosphorylation site required for STAT3 activation and nuclear translocation, was analysed across renal control tissues, primary ccRCC tumours, and metastatic ccRCC samples using the QF-Pro® assay. The quantitative

analysis demonstrated a progressive increase in STAT3 activation from noncancerous renal tissue to metastatic tumours. Renal control tissues showed minimal activation, while primary ccRCC samples exhibited a modest but statistically significant increase. Furthermore, metastatic ccRCC samples showed a marked elevation in STAT3 activation, highlighting the role of Tyr705-STAT3 phosphorylation in tumour progression and aggressiveness (Figure 4).

These results underscore the potential of STAT3 activation as a biomarker for ccRCC prognosis, with higher activation correlating with more advanced disease stages and poorer patient outcomes.

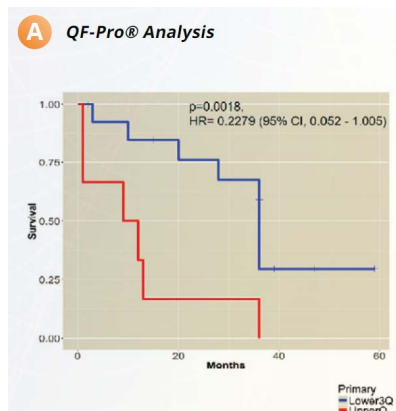
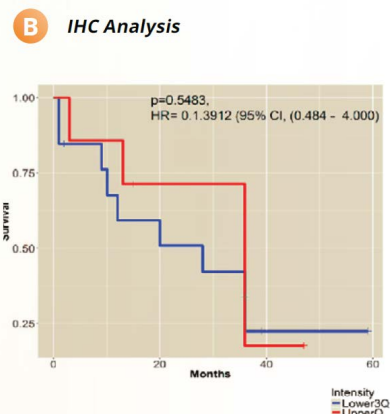


Figure 3: Akt/PKB activation state correlates with poor overall survival in ccRCC. Kaplan-Meier survival outcomes related to PKB/Akt activation as determined by QF-Pro® (A) or by conventional IHC (B).

A) QF-Pro® analysis revealed significantly poorer survival for patients in the upper quartile compared to the lower three quartiles.



B) No significant survival difference was observed using conventional IHC.

Features

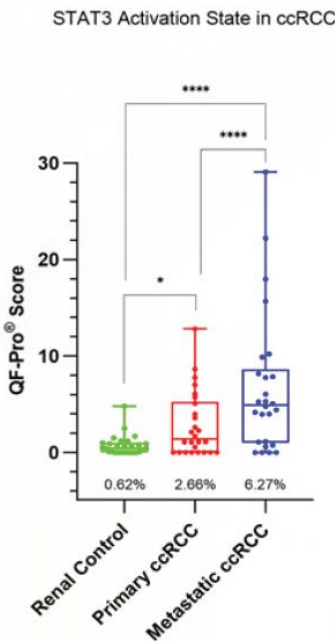


Figure 4: Tyr705 activation is higher in metastatic ccRCC tumours in FFPE TMAs. Box and Whisker plots show the QF-Pro® scores of the three groups. Activation of Tyr705 is higher in metastatic cores than in primary cores. Both groups are significantly higher than the non-cancerous renal control tissue ($p < 0.001$).

4. Conclusion

QF-Pro® technology represents a significant advancement in prognostic biomarker analysis by enabling the precise measurement of protein activation states rather than simple expression levels. This is a paradigm shift from traditional methods such as IHC, which are limited to detecting protein expression without assessing functionality.

By focusing on post-translational modifications, such as phosphorylation, QF-Pro® offers unparalleled specificity and sensitivity, revealing critical insights into the signalling dynamics that drive tumour progression.

In the context of ccRCC, QF-Pro® has shown clinical utility by accurately assessing the activation states of two key biomarkers, PKB/ Akt and STAT3. This technology offers valuable prognostic insights, linking biomarker activation to tumour progression and patient outcomes.

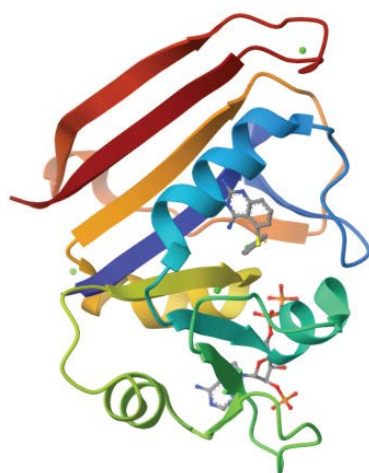
By integrating multiple biomarkers, QF-Pro® enhances risk stratification and supports personalized treatment strategies. With its ability to measure functional protein states and monitor therapeutic responses, QFPro® addresses the limitations of conventional approaches, paving the way for more precise and individualized cancer care in ccRCC.

References

1. Miles J, Applebee CJ, Leboucher P, et al. Time resolved amplified FRET identifies protein kinase B activation state as a marker for poor prognosis in clear cell renal cell carcinoma. *BBA Clin.* 2017;8:97-102. doi:10.1016/j.bbaci.2017.10.002
2. Veeriah S, Leboucher P, de Naurois J, et al. High-throughput time-resolved FRET reveals Akt/PKB activation as a poor prognostic marker in breast cancer. *Cancer Res.* 2014;74(18):4983-4995. doi:10.1158/0008-5472.CAN-13-3382



A novel platform for functional biomarkers



Protein-Small Molecule Biomolecular Interactions – a Retrospective

Surface Plasmon Resonance (SPR) is an invaluable technique that generates information rich data for a variety of biomolecular interactions. Researchers utilize SPR to understand biological pathways and to develop and characterize a range of potential therapeutics to treat disease and illnesses. These interactions include those occurring with and between the major classes of biological macromolecules. However, this article is focused solely on using SPR to study biomolecular interactions involving small molecules binding to proteins.

To provide key information about these interactions, many researchers are relying on SPR, which is a widely used technique for the determination of kinetics and thermodynamics.

“Small molecules” for purposes of this article generally refers to molecules with molecular weights of about 1,000 Da or less. There are certain standard approaches that researchers follow to carry out these types of experiments. Since a higher surface density is needed when there is a large molecular weight difference between the protein (target) and “small molecule” (analyte) whose interaction is being studied, direct coupling is usually the preferred means of attaching a

target to the sensor chip. Of necessity, since many “small molecules” do not contain primary amines or thiol groups needed for direct coupling, the protein is usually coupled to a hydrogel surface (typically dextran) and then the small molecule analyte is injected over the surface at 5 or more concentrations and kinetics are determined. If testing is done at multiple temperatures, thermodynamics can also be determined. Since it is common for small molecules to show limited solubility in the aqueous running buffers used for SPR studies (eg. PBS, HEPES), analytes soluble in DMSO are typically diluted with running buffer to about 1-5% DMSO prior to SPR analysis. In some cases, detergents may also be used to help with solubility issues. Many of these experiments are carried out to aid in the development of small molecules as potential therapeutics for disease.

Here are highlighted some recent research articles where the Reichert’s SPR systems have been utilised for investigating low molecular weight molecules interactions with proteins.

Example 1. Target HIV – using a Reichert4SPR for screening

A 2019 article in ACS Infectious Diseases highlights how some of the unwanted functions of HIV Nef accessory protein, which plays a key role in HIV replication, can be blocked by small molecules¹.

For the results presented in this article, researchers developed analogues to an earlier small molecule that showed promise in testing. They had more than 200 analogues to analyse and ranked them based on binding results obtained using a Reichert4SPR system. Recombinant HIV-1 Nef was covalently bound to a dextran sensor chip as the target and binding interactions with the analogues were ranked in terms of affinity, residence time and binding response¹.

Of the 216 analogues screened, 45 exhibited no binding. The remainder of the responses were ranked based on the magnitude of the responses, their kinetics, including on- and off- rates, and activity from a separate assay¹.

SPR results for the two compounds shown below are representative of how the researchers determined that the benzimidazole moiety at position C is essential for Nef inhibitor action.

As noted in the article, the percent inhibition of HIV-1 infectivity determined using the TZM-bl reporter cell assay goes down by nearly 90% if the benzimidazole moiety at position C (highlighted in green below) is not present on the scaffold.

In addition, the affinity of the interaction decreases significantly from 13 nM to 9.8 μ M¹ and the absolute magnitude of the responses decreases approximately fourfold (overlays shown below). Based on these results, FC-8698 was ranked as one of the top overall binders of the compounds studied.¹

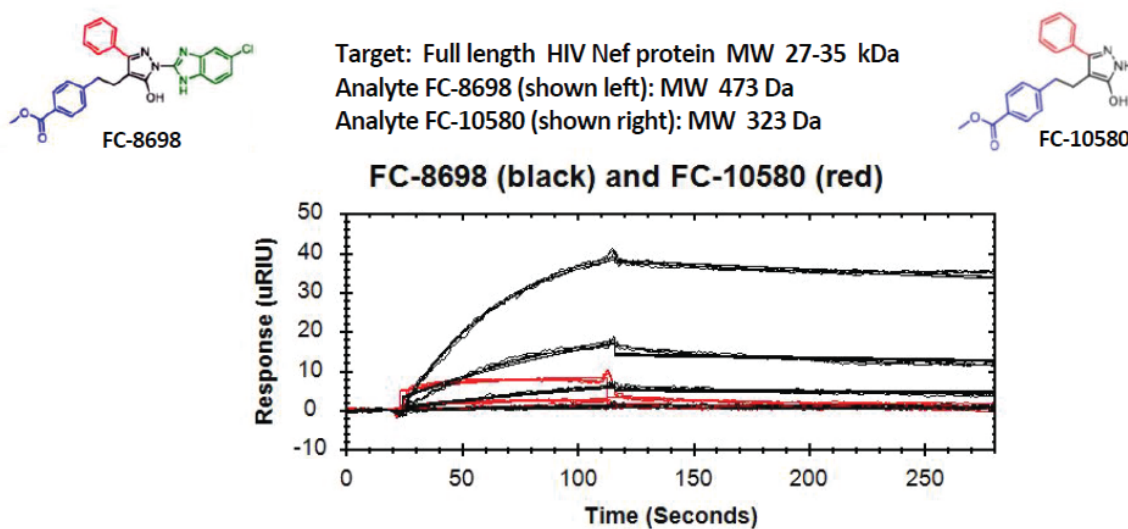


Figure 1: Overlaid sensorgrams show binding of analyte FC-8698 (black) containing the benzimidazole moiety (green section on structure on left) and binding of analyte FC-10580 (red) with the same backbone but without the key group. Using SPR, the KD for FC-8698 was determined to be 13 nM vs the KD of 9.8 μ M for FC-10580. In both cases, binding is to recombinant HIV-1 Nef and curves were fit using a 1:1 binding model.

Example 2: Target Tuberculosis – using a 2-channel Reichert SPR for initial screening

A 2017 article in ChemMedChem describes how a SR7500DC (2-channel Reichert SPR instrument) has been used for the screening of potential antimycobacterial agents against *Mycobacterium tuberculosis* (Mtb)². In this article, researchers explain that there is an urgency to their work because multi-drug resistance and the need for long term treatment are making it difficult to treat this disease and, they note that there are millions of new cases of Mtb infections each year worldwide (as of the year 2017 when they wrote their article)². Previous work showed that the enzyme CYP121 is essential for Mtb growth making it a potential target for Mtb treatment.²

Screening in this study was carried out based on biophysical and microbiological methods. The initial screen was carried out using Surface Plasmon Resonance (SPR) with a Reichert 2-channel instrument and involved capturing biotinylated CYP121 on a

streptavidin chip as the target and then analysing binding to the target of 139 novel small molecule antimycobacterial compounds across six classes.

Researchers built up small molecule compounds on six different scaffolds to probe a wide range of structures. Of the compounds screened, 32% showed a response using SPR. Seventeen of the compounds had higher responses than econazole, the positive control. When compared to the positive control econazole, forty-four of the compounds screened were found to be worthwhile for further testing (i.e. to have responses R/R_{pos} of 0.5 or higher). Further testing with multiple techniques led the researchers to a promising target for further research, a compound they call I:47 which exhibited good antimycobacterial activity and bacterial selectivity with a favourable toxicity profile².

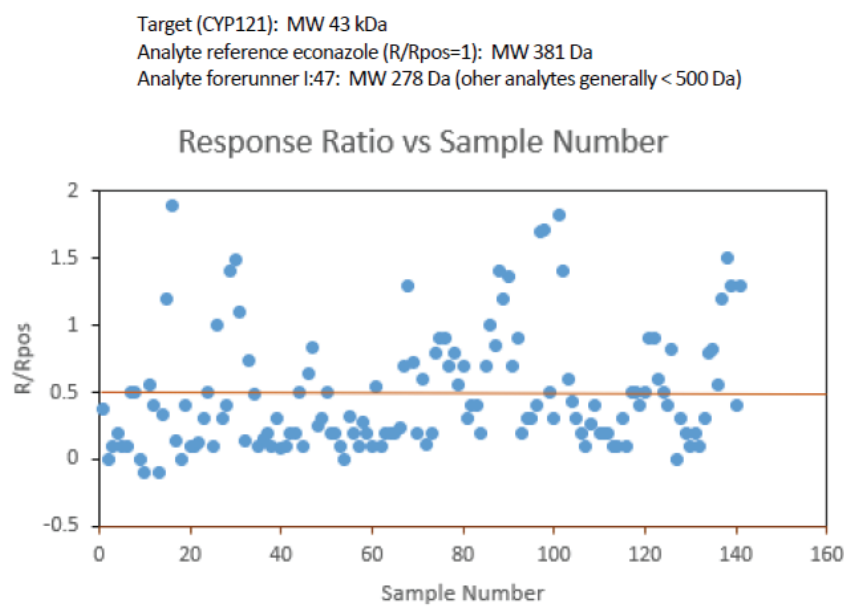


Figure 2: SPR was used to do an initial screen of 139 novel small molecule inhibitors and differentiate between binders and non-binders. In addition, the size of the response was compared to the response for the positive control, econazole ($R(\text{analyte})/R(\text{econazole})$). The reddish line at 0.5 differentiates between analytes that were carried forward ($\text{ratio} > 0.5$) and the remainder that were dropped from further testing.

Example 3: Anti-Cancer Drug Candidates – comparison using a Reichert4SPR

A 2017 Article in PLOS 1 includes SPR data obtained using a Reichert4SPR for the binding of small molecule anti-cancer drugs to human serum albumin (HSA)³. In this study, researchers looked at two potential anti-cancer drug candidates, NSC48693 (which is hydrophilic) and NSC290956 (which is hydrophobic) and determined where they bind to HSA using fluorescence quenching and molecular modelling. For information regarding the kinetics and thermodynamics of the small molecule/HSA interactions, researchers used a Reichert4SPR.

HSA was amine coupled to a dextran sensor chip and then the two drug candidates were diluted and injected over the surface as analytes. Kinetic analysis resulted in the determination of the affinity for the HSA/NSC48693 interaction ($K_D = 13.8 \mu\text{M}$) to be almost 10 times higher than the affinity for the HSA/NSC290956 interaction ($K_D = 116 \mu\text{M}$).³ This information is expected to be particularly useful in later determination of the type of dosing that would be needed for clinical studies using each compound.

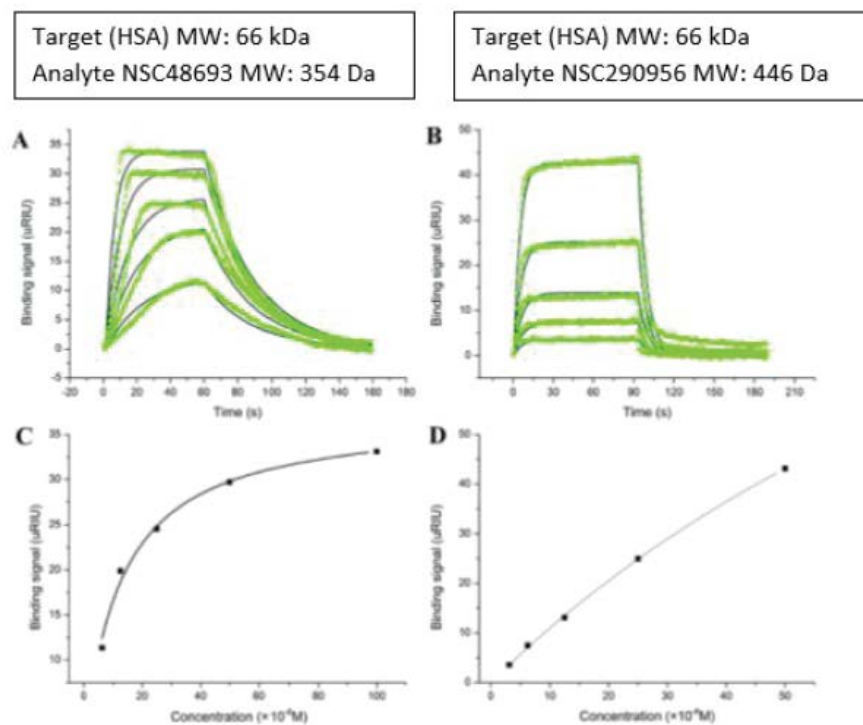


Figure 3: A and C (left) show the overlaid sensorgrams (with fit to 1:1 model in green) and Langmuir isotherm plot, respectively, for the HSA/NSC48693 interaction ($K_D = 13.8 \mu\text{M}$). B and D (right) show the overlaid sensorgrams (with fit to 1:1 model in green) and Langmuir isotherm plot, respectively, for the HSA/ NSC290956 interaction ($K_D = 116 \mu\text{M}$).

Example 4: Development of CK2 inhibitors for Cancer Treatment

In a 2019 article in the Journal of Medicinal Chemistry, researchers used the protein kinase CK2 as target and looked for potential inhibitors⁴. The protein kinase CK2 is known to play an important role in pro-oncogenic pathways that are critical to cells including proliferation, differentiation, and survival. Previous research involving development of inhibitors for the protein kinase CK2 were targeted toward the ATP binding pocket, but it was found that the compounds developed could also act on other targets in the body with ATP binding pockets which could then cause unwanted side effects. Researchers in this study previously determined there was a more specific, potentially druggable site on the protein CK2.

In their current work they sought to prove it to be a viable option by developing 2-Aminothiazole Derivatives that they could test. Researchers' amine coupled Anti-GST to the surface of a dextran sensor chip and then captured GST-tagged CK2 α over the surface as a target for the allosteric inhibitors they made⁴. Of the allosteric inhibitors they constructed and tested, they found one of the compounds, 2 hydroxy-4-((4-(naphthalen-2-yl)thiazol-2-yl) amino)benzoic acid to be the lead compound with a sub-micromolar IC₅₀. Testing was carried out using a number of techniques including SPR⁶. Comparing IC₅₀ (biochemical inhibition) results with SPR binding affinity constants obtained with a 2-channel Reichert SPR for a number of the inhibitors they tested, they found good agreement⁵.

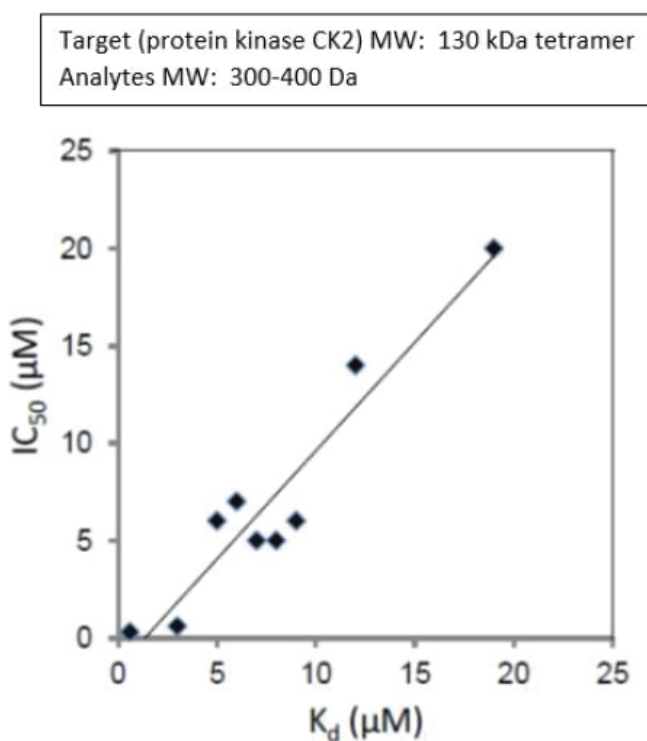


Figure 4: Good correlation is seen between IC₅₀ results obtained for a number of allosteric inhibitors binding to CK2 and KD results obtained for the same biomolecular interactions using SPR. Values are in μM.⁵

Features

Example 5: Small molecule zinc complexes binding to DNA

In a 2015 article in Dalton Transactions, researchers designed small molecule zinc complexes and determined how they fit into bulges and quadruplexes on DNA. Non-canonical nucleobases that are part of DNA bulges are common targets when designing small molecules for binding both organic and inorganic compounds. And Zn(II) complexes containing planar aromatic pendants with two fused rings bind to DNA Hairpin (T-bulge) more tightly than complexes with nonplanar pendants.⁶ Both a better understanding of these types of interactions and the development of alternative ways to recognize unusual nucleic acid structures could lead to improved design of small molecules for future therapeutic applications.

Researchers in this study used Reichert's 2-channel surface plasmon resonance (SPR) system to capture biotinylated DNA oligos on a planar streptavidin chip. They then flowed over the analytes at various concentrations to characterize the binding of Zn complexes to DNA T-bulge and T-loop structures.⁶ An example of a typical result is shown here:

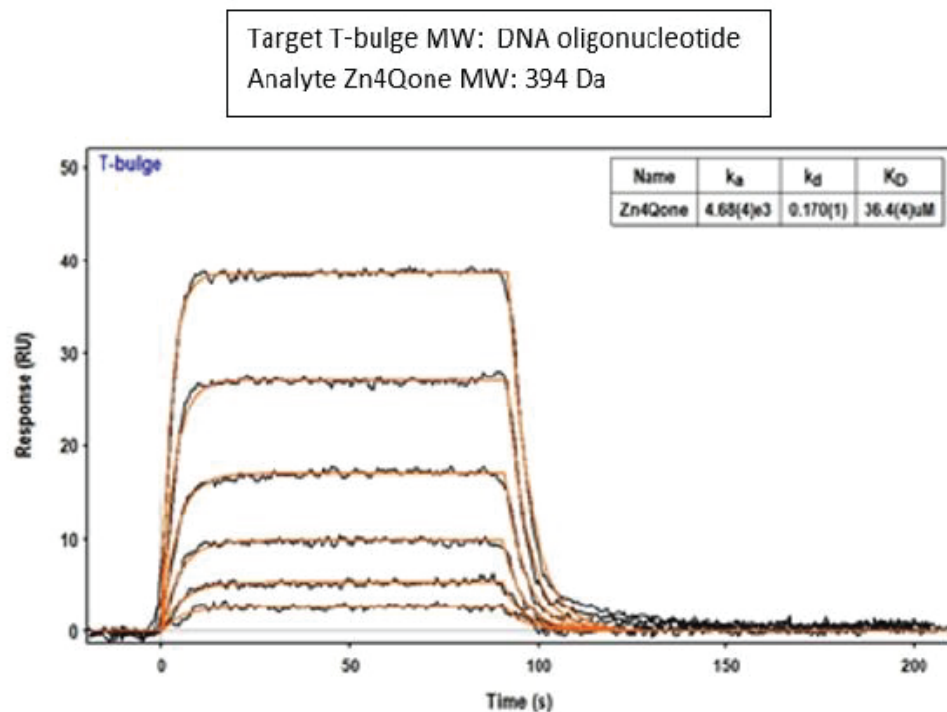


Figure 5: Sensorgrams for Zn4Qone binding to T-bulge are shown. The global best fit is to a 1:1 binding model with a KD value of 36.4 μ M.

Conclusion

SPR can play a pivotal role in therapeutics development with the characterization of small molecule interactions with proteins. Reichert's SPR systems have been implemented in a variety of research applications (<https://www.reichertspr.com/publications/>) and have the sensitivity and performance characteristics to meet challenging experimental needs such as low molecular weight interaction analysis. Reichert offers three SPR platforms, 2SPR, 3SPR and 4SPR systems that are affordable, flexible and have outstanding performance.

References

1. Shi H, Tice CM, Emert-Sedlak L, Chen L, Li WF, Carlsen M, Wrobel JE, Reitz AB, Smithgall TE. Tight-Binding Hydroxypyrazole HIV-1 Nef Inhibitors Suppress Viral Replication in Donor Mononuclear Cells and Reverse Nef-Mediated MHC-I Downregulation. *ACS Infect Dis.* 2020 Feb 14;6(2):302–312. doi: 10.1021/acsinfecdis.9b00382. Epub 2019 Dec 16. PMID: 31775511.
2. Christian Brengel, Andreas Thormann, Alexander Schifrin, Giuseppe Allegretta, Ahmed A. M. Kamal, Jçrg Haupenthal, Isabell Schnorr, Sang Hyun Cho, Scott G. Franzblau, Martin Empting, Jens Eberhard, and Rolf W. Hartmann, "Biophysical Screening of a Focused Library for the Discovery of CYP121Inhibitors as Novel Antimycobacterials," *ChemMedChem*, 2017, 12, 1616 – 1626. DOI: 10.1002/cmdc.201700363
3. Chuanbo Liu, Zuoja Liu and Jin Wang, "Uncovering the molecular and physiological processes of anticancer leads binding human serum albumin: A physical insight into drug efficacy," *PLOS ONE* April 20, 2017. doi.org/10.1371/journal.pone.0176208.
4. Benoît Bestgen, Irina Kufareva, Weiguang Seetoh, Chris Abell, Rolf W. Hartmann, Ruben Abagyan, Marc Le Borgne, Odile Filhol, Claude Cochet, Thierry Lomberget and Matthias Engel, "2-Aminothiazole Derivatives as Selective Allosteric Modulators of the Protein Kinase CK2. 2. Structure-Based Optimization and Investigation of Effects Specific to the Allosteric Mode of Action," *J. Med. Chem.* 2019, 62, 1817–1836, DOI: 10.1021/acs.jmedchem.8b01765
5. Reprinted (adapted) with permission from *J. Med. Chem.* 2019, 62, 1817–1836, Publication Date: Feb 1, 2019, DOI: 10.1021/acs.jmedchem.8b01765. Copyright © 2019 American Chemical Society.
6. Kevin E. Sitors, Stephanie A. Sander, Jason R. Devlin, and Janet R. Morrow. "Bifunctional Zn (ii) complexes for recognition of non- canonical thymines in DNA bulges and G-quadruplexes." *Dalton Transactions*, 2015, Vol 44, pp. 3708–3716.





Inside BioArtha Labs: Leadership, Science, and the Business of Innovation

Mr. Ganesh

co-founder, BioArtha Labs takes us through its journey, why indigenization is more than just buzzword and his views on where Indian biotech is headed.

Mr. Ganesh co-founded BioArtha Labs in 2021 with a simple yet profound vision: to create something of value, despite limited capital or infrastructure. “There was no grand plan, just a strong urge to start, to build, to do something that was ours.”

Mr. Ganesh’s journey reflects not just academic milestones but also emotional investment in science. With a master’s degree in Biochemistry from Mysore University, and several years of dedicated research in protein chemistry at CFTRI, Mysore, his path was anything but conventional!

“Our lab, though based in a food institute, was intensely focused on classical protein chemistry—right from structural restoration to sequencing,” he recalls. “We did everything manually in the early days—protein and DNA sequencing by hand, until the first RT-PCR machines arrived, massive and manual, marking the technological leap we witnessed firsthand.

This leap coupled with industry experience in diagnostics and food applications and a deep-rooted scientific spirit, laid the foundation of BioArtha Labs.”

Q. What is the driving mission behind BioArtha Labs, and how does it align with the current needs of the biopharma industry?

See, what we felt was, as Indians, we know how to do things. The skill is there. The only thing that is sometimes lacking, especially in our field—is the support or access to the kind of capital needed to really push innovation. Both me and my co-founder realised that there are so many researchers who want reliable products—homegrown—technologies that are available in India and suited to our needs. So, that became our mission—Indigenization. Internalising technology, making sure these solutions are built here, in India, for

Indian researchers. That’s what we set out to do.

Q. How did you identify the gap in the biopharma industry that BioArtha could fill?

Right now, a large portion of Biotech—maybe 70 to 80%—is dependent on foreign multinationals, across reagents, technologies and equipment. We saw an opportunity here. China has already done this—localised and scaled their manufacturing!

We felt India could do the same, especially in biopharma and diagnostics, just like we did in APIs and generics. The big difference is, China has a robust supply chain

Interview

and support system. We don't-yet.

We identified our four key areas where there is heavy dependence on imports, and we've spent time developing these products ourselves and understanding what the industry needs. We have also diversified across categories. So yes, we have come far, but there is still more to do!

Q. One of your services include recombinant DNA strain engineering and antibody development. How do these offerings translate to real-world applications?

Currently, biology revolves around small molecules and proteins- be it for therapeutics, vitamins or even sugar alternatives. But India isn't self-reliant in these areas. Like I said, we are still importing basic chemicals like amino acids and even Stevia.

Fermentation is a game-changer here. Microbes can make everything- from vitamins to milk proteins, to even bio-based alternatives like bioplastics and cultured meat. Our strengths lie around this- genetic modifications, biotransformation and precision fermentation. When we realised the demand, we expanded our services to include making vitamins D, B12, terpenoids and even aroma molecules like sandalwood alternatives. It's about creating indigenous and sustainable solutions-because the world is finally noticing Indian innovation, and we make sure our products truly reflect that.

Q. With precision being so crucial in today's age, how does it shape the workflow at BioArtha Labs?

Since we supply to biopharma, we're bound by regulatory standards- so precision isn't optional, it's essential. We are ISO 13485 certified for medical device manufacturing, which already sets a high bar. We have built a culture where precision is second nature. We are still learning and working towards Kaigen-level consistency.

Q. Earlier, you mentioned how you used to do things manually- how have those technologies or methodologies evolved and where do you see the trend heading now?

“
It's about creating indigenous and sustainable solutions-because the world is finally noticing Indian innovation
”

Things are moving really fast-especially in precision fermentation. Earlier, hitting 80-100 OD was a big deal, now we're easily touching 250-270. With real-time data on things like CO_2 and by-products, we can optimise was better and cut down on the number of fermentations. Even analytical tools like HPLCs have advanced and become a bit more affordable too. Antibody generation has evolved from hybridomas to phage display, drastically reducing turnaround time. Techniques like Gibson assembly now let us do in a day what once took months. Gene synthesis is faster and cheaper and skilled manpower is more readily available. Regarding AI, it is going to disrupt biology, but not without human intelligence. AI has been in biotech for years, but now it's about using it meaningfully alongside experience. We'll be there to see how truly it transforms!

Q. You mentioned biosimilars earlier when we spoke about how you started. How do you see them shaping the future of therapeutics? And with monoclonal antibodies- it feels like every time the FDA announces a new approval, it's always another monoclonal. Why do you think that's the case?
A lot of therapeutic monoclonal antibodies are going off-patent. For example, the blockbuster Humira is set to go off in 2026 maybe, and pretty much every major company is working on biosimilars for it. It is going to be a big disruptor in the therapeutics space.

And now, with CAR-T therapies also coming up, the whole world is moving fast. This disruption is especially

Interview

relevant for India-because biosimilars offer a much more affordable alternative and with insurance penetration slowly increasing, access is improving. But India's a different beast altogether when it comes to scale- everything has to be massive.

BioArtha Labs is involved too – not directly but indirectly- we manufacture some of the key reagents/enzymes that go into the production process. We are a part of that ecosystem, and we see huge opportunities. I think by 2030, we will see a very different landscape, with more India biosimilars getting approved.

“
Regarding AI, it is going to disrupt biology, but not without human intelligence
”

Q. Lastly, I am curious to know – BioArtha Labs started in 2021, how did Covid affect you?

(laughs) Honestly, by the time we really got going during COVID, we were already into the second or third wave. It was tough to get into the pandemic space by then. There were already big players in the game, prices had dropped, and we made a conscious decision not to jump into it. In hindsight, I think that was the right call. It was like the wild west of biotech back then-but if something like that were to happen again, we'll be ready. We are confident we can support our nation with production capabilities and not depend on China. We will be there, yes.



“
This disruption is especially relevant for India-because biosimilars offer a much more affordable alternative and with insurance penetration slowly increasing, access is improving
”



Freeze drying of beads containing yeasts

BUCHI Lyovapor™ L-200 Pro Facilitates Precision Freeze Drying of Yeast-Loaded Microcapsules for Long-Term Storage

This application outlines a robust methodology for the preservation of *Saccharomyces cerevisiae* via encapsulation and freeze drying. Yeast suspensions, pre-treated with trehalose and skimmed milk as lyoprotectants, were processed using the BUCHI Encapsulator B-390 to generate uniform microbeads, which were flash-frozen in liquid nitrogen. Subsequent lyophilization with the Lyovapor™ L-200 Pro preserved bead morphology and facilitated high post-rehydration viability. SEM imaging confirmed structural integrity and differentiation between protective matrix and cellular content. This process offers a scalable and reproducible platform for stabilizing microbial formulations with high flowability and fast reconstitution—ideal for applications in probiotics, bioprocessing, and microbial starter cultures.

Keywords or phrases: Freeze drying, *Saccharomyces cerevisiae*, microorganisms, lyoprotectants

Introduction

Freeze drying or lyophilisation is a very well-known dehydration method commonly used to preserve microorganisms, food or pharmaceuticals such as protein-based drugs. It can create high quality final dry products by combining freezing and drying in a unique operation¹.

Freeze drying is regularly used to preserve microbial culture collections^{2,3} since it offers nonnegligible advantages such as the convenience of storage and the possibility to transport the microorganisms by mail⁴. Moreover, the product only requires low maintenance, the cultures are protected from contamination during storage and the microorganisms remain viable for long periods of time².

It is however common knowledge that freeze drying is critical for microorganisms as it affects both their viability and physiological state negatively¹. A large

Application Showcase

variety of survival rates can be found depending on methods and organisms; viability levels are however significantly lower than for liquid nitrogen storage². The observed decrease in viability is mainly due to some undesirable side effects such as the formation of ice crystals within the cells¹, the denaturation of sensitive proteins or some irreversible changes in the physical state of the membrane lipids during the process^{3,5}. In order to prevent such effects, protective substances such as skim milk, sucrose, glycerol, DMSO or trehalose are commonly used before freezing or freeze drying^{1,3}.

Trehalose is reported to exert a protective effect on yeasts and bacteria under extreme environments such as desiccation, freezing, osmotic stress and heat shock. Those protective effects are linked to the stabilization of membranes and the preservation of enzyme activity.

Several hypotheses concerning trehalose protective effects have been reported. Some reports assume it acts by replacing water molecules involved in the maintenance of the tertiary structure of proteins through multiple external hydrogen bonds, others that it forms glassy structures which assure physical stability; special interactions at molecular level therefore probably have to operate to assure physical stability^{3,6}.

Next to fermentation processes or transformation of foods, microorganisms such as *Saccharomyces cerevisiae* or lactic acid bacteria are of economic importance in the field of probiotic dietary food and feed supplements. These applications however require the preservation of cell viability during storage⁷. By combining granulation and freeze drying, dust free particles homogeneous in size and composition can be obtained. This will enable a good particle flowability, an easier dosage and a faster reconstitution of the product due to a higher surface area. Despite the above challenges, freeze drying remains a convenient method of preserving yeasts, sporulating fungi and bacteria since the long- term viability remains usually rather good and the requirements for storage and distribution of the strains are quite simple⁸.

This application note therefore aims to produce *Saccharomyces cerevisiae* particles as a model microorganism using the Encapsulator B-390 as a granulator to prill the yeasts suspension into liquid nitrogen and form monodispersed beads that will then be freeze dried using the Lyovapor™ L-200.

Experimental

1. Equipment

- » Biosafety Cabinet Class II
- » BUCHI Encapsulator B-390
- » BUCHI Lyovapor™ L-200 Pro
- » BUCHI Lyovapor™ Software
- » BUCHI Lyovapor™ Drying chamber with heatable shelves

2. Chemicals

- » YPD Medium, Sigma Aldrich
- » Trehalose, Sigma Aldrich
- » Skimmed milk powder
- » Agar
- » Deionized water
- » Liquid nitrogen

3. Materials

- » Glass petri dishes
- » Benchtop liquid nitrogen container

4. Method

The work described in this application note was performed under aseptic conditions. 84 g of commercially available baker's yeast were suspended in 50 mL of sterile YPD Medium (Sigma Aldrich). 50 mL of sterile lyoprotectant medium containing 5 g of trehalose (Sigma Aldrich) and 5 g of skimmed milk in deionized water was then added to the yeast suspension before extrusion with the Encapsulator B-390 (Table 1). The extruded droplets were collected and frozen in a liquid nitrogen bath before being transferred in stainless steel trays and stored in a -25 °C freezer until freeze drying.

Application Showcase

Parameter	300 µm nozzle	1 mm nozzle
Frequency [Hz]	680	60
Electrode [V]	750	2500
Pressure [mbar]	500	500

Table 1: Encapsulation parameters

The freeze-drying steps (primary and secondary drying) were programmed using the Lyovapor™ Software as listed in Table 2. The Lyovapor™ L-200 Pro was used with the drying chamber with heatable shelves and ambient air.

Step	1	2	3	4
Phase	Primary drying	Primary drying	Secondary drying	Secondary drying
Duration	02:00	20:00	02:00	04:00
Shelf temperature	-35.0	-15.0	-15.0	30.0
Shelf temperature gradient	0.17	0.00	0.38	0.00
Pressure zone	Regulated	Regulated	Regulated	Regulated
Pressure	0.200	0.200	0.200	0.200
Safety pressure	0.500	0.500	0.500	0.500
Safety pressure duration	10	10	10	10

Table 2: Parameters of the primary and secondary drying

The beads without yeasts were prepared using the same media composition and the same parameters as the beads containing yeasts.

After freeze drying, 1 mL of sterile water was added to 1 mL of beads in order to reconstitute the sample. For the bead containing yeasts, serial dilution of 10x, 100x and 1000x were performed for each reconstituted solution. The reconstituted solution and the dilutions were then plated on YPD agar plate as shown in Figure 1. The agar plate were then incubated at 28 °C for 24h to evaluate cell viability.

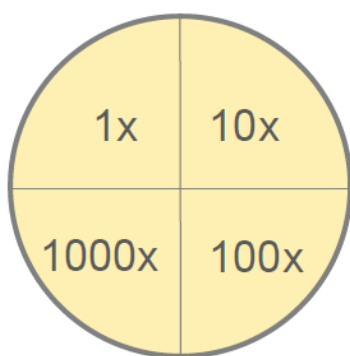


Figure 1: Yeast viability test on agar plate

Result and discussion

Microbeads containing yeasts can be produced by extruding a mixture made of yeasts and lyoprotectant medium in liquid nitrogen, using the Encapsulator B-390. Results showed that yeasts could be granulated by dripping it in liquid nitrogen with the Encapsulator B-390; beads of around 700 µm and 1500 µm were produced with the 300 µm nozzle and the 1 mm nozzle respectively. Similar results were obtained using solution containing lyoprotectant medium only.

As shown in Figure 2, after lyophylisation the beads remained similar in shape and size than the wet frozen beads.



Figure 2: Yeast microbeads produced with the Encapsulator B-390 and the 300 µm nozzle before (top) and after (bottom) freeze drying.

The analysis of the bead structure was performed through SEM microscopy. In Figure 3, a difference in beads morphology can be observed between beads containing yeasts (bottom) and beads made of lyoprotectant medium only (top). The beads containing yeasts exhibit a rough structure made of 5 µm agglomerated particles that can be assumed to be the microorganisms, while the beads containing only lyoprotectant have a smoother structure.

Application Showcase

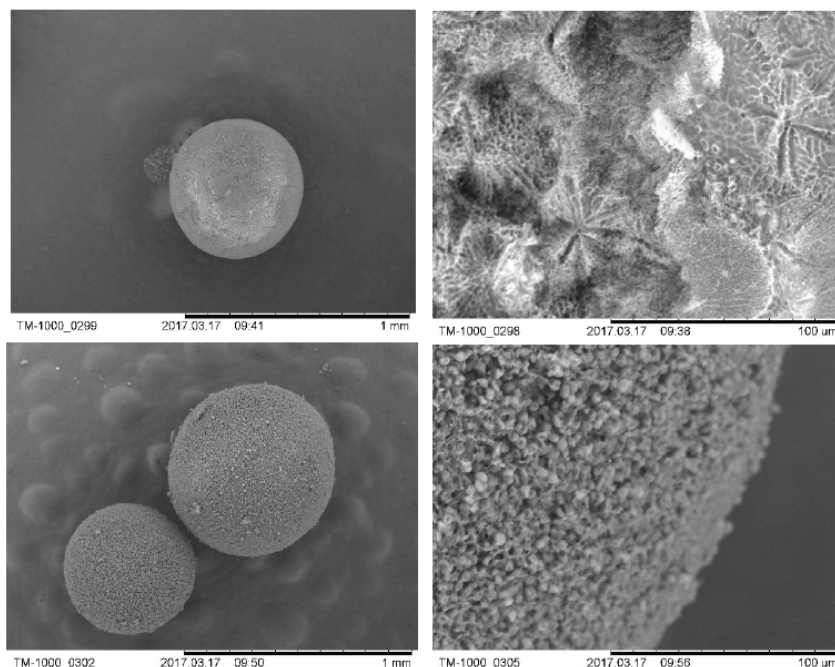


Figure 3: Structure comparison of freeze-dried beads with (bottom) and without (top) yeasts.

When subjected to freeze drying, biological systems can be damaged due to changes in the physical state of the lipids in the membrane or due to changes in the structure of some proteins ^{3,9}.

In order to verify yeast viability, the yeasts were rehydrated, diluted and incubated on YPD-agar plate at 28 °C for 24 hours. Figure 4 confirms literature reports showing that despite a loss of viability, yeast can still grow after lyophilisation ^{2,4,6,10}.

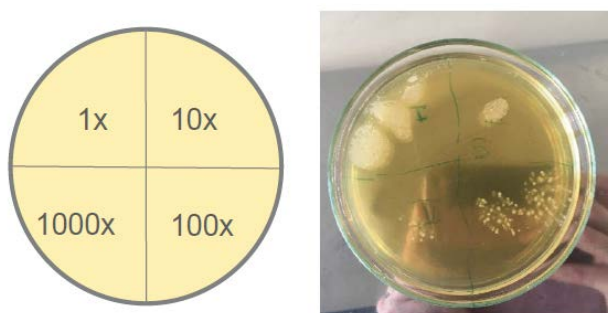


Figure 4: Yeast viability on agar plate after 24h incubation at 28°C

Conclusion

Yeast beads could easily be produced with the Encapsulator B-390 and freeze dried using the Lyovapor™ L-200. Beads of 700 μm and 1500 μm diameter were obtained using the B-390 with the 300 μm and 1000 μm nozzle, respectively. No change in size and shape of the beads were observed after freeze drying. The granules had a good flowability and dosage was easily done, moreover the particles were rapidly dissolved when mixed with water. The microorganisms still kept a good viability during storage after lyophilisation and could successfully be grown again after rehydration.

The combination of granulation and freeze drying in this application showed promising results. It can open new possibilities in fields such as fermentation processes and food transformation to produce culture starters that can easily be dosed and reconstituted or in the field of probiotics and food supplements to obtain a dust free, free flowing powder with homogeneous particle size and particle composition.

Application Showcase

References

1. N'Guessan, F. K.; Coulibaly, H. W.; Alloue-Boraud, M. W. A.; Cot, M.; Djè, K. M. Production of Freeze-Dried Yeast Culture for the Brewing of Traditional Sorghum Beer, Tchapalo. *Food Sci. Nutr.* 2016, 4 (1), 34–41.
2. Bond, C. Freeze-Drying of Yeast Cultures. In *Cryopreservation and Freeze-Drying Protocols*; Day, J., Stacey, G., Eds.; *Methods in Molecular Biology*TM; Humana Press, 2007; pp 99–107.
3. Leslie, S. B.; Israeli, E.; Lighthart, B.; Crowe, J. H.; Crowe, L. M. Trehalose and Sucrose Protect Both Membranes and Proteins in Intact Bacteria during Drying. *Appl. Environ. Microbiol.* 1995, 61 (10), 3592–3597.
4. Miyamoto-Shinohara, Y.; Imaizumi, T.; Sukenobe, J.; Murakami, Y.; Kawamura, S.; Komatsu, Y. Survival Rate of Microbes after Freeze-Drying and Long-Term Storage. *Cryobiology* 2000, 41 (3), 251–255.
5. Wolkers, W. F.; Tablin, F.; Crowe, J. H. From Anhydrobiosis to Freeze-Drying of Eukaryotic Cells. *Comp. Biochem. Physiol. A. Mol. Integr. Physiol.* 2002, 131 (3), 535–543.
6. Lodato, P.; Huergo, M. S. de; Buera, M. P. Viability and Thermal Stability of a Strain of *Saccharomyces Cerevisiae* Freeze-Dried in Different Sugar and Polymer Matrices. *Appl. Microbiol. Biotechnol.* 1999, 52 (2), 215–220.
7. Strasser, S.; Neureiter, M.; Geppl, M.; Braun, R.; Danner, H. Influence of Lyophilization, Fluidized Bed Drying, Addition of Protectants, and Storage on the Viability of Lactic Acid Bacteria. *J. Appl. Microbiol.* 2009, 107 (1), 167–177.
8. Miyamoto, T. (Kyushu U.; Kawabata, K.; Honjoh, K.; Hatano, S. Effects of Trehalose on Freeze Tolerance of Baker's Yeast. *J. Fac. Agric. – Kyushu Univ. Jpn.* 1996.
9. Giulio, B. D.; Orlando, P.; Barba, G.; Coppola, R.; Rosa, M. D.; Sada, A.; Prisco, P. P. D.; Nazzaro, F. Use of Alginate and Cryo-Protective Sugars to Improve the Viability of Lactic Acid Bacteria after Freezing and Freeze-Drying. *World J. Microbiol. Biotechnol.* 2005, 21 (5), 739–746.
10. Cerrutti, P.; Huergo, M. S. de; Galvagno, M.; Schebor, C.; Buera, M. del P. Commercial Baker's Yeast Stability as Affected by Intracellular Content of Trehalose, Dehydration Procedure and the Physical Properties of External Matrices. *Appl. Microbiol. Biotechnol.* 2000, 54 (4), 575–580.



BUCHI

Lyovapor™
L-200 Pro

Autoclaves (Vertical Type)

Microprocessor control with reliable safety functions guarantees optimum sterilization temperature

Features

- ◆ **Microprocessor controller and temperature calibration function allows for high precision temperature control**
 - Sterilization temperature at 110 to 123°C
 - Melting* temperature at 60 to 100°C

* Liquefaction of coagulated agar media.
- ◆ **Automatic sterilization system for unattended operation**
 - Heating > Check safe > Sterilization > Sterilization safe > Exhausting > End
- ◆ **Convenient operation modes for various uses**
 - Standard modes and program modes are listed in detail as below tables.
- ◆ **Temperature calibration function**



Available capacities

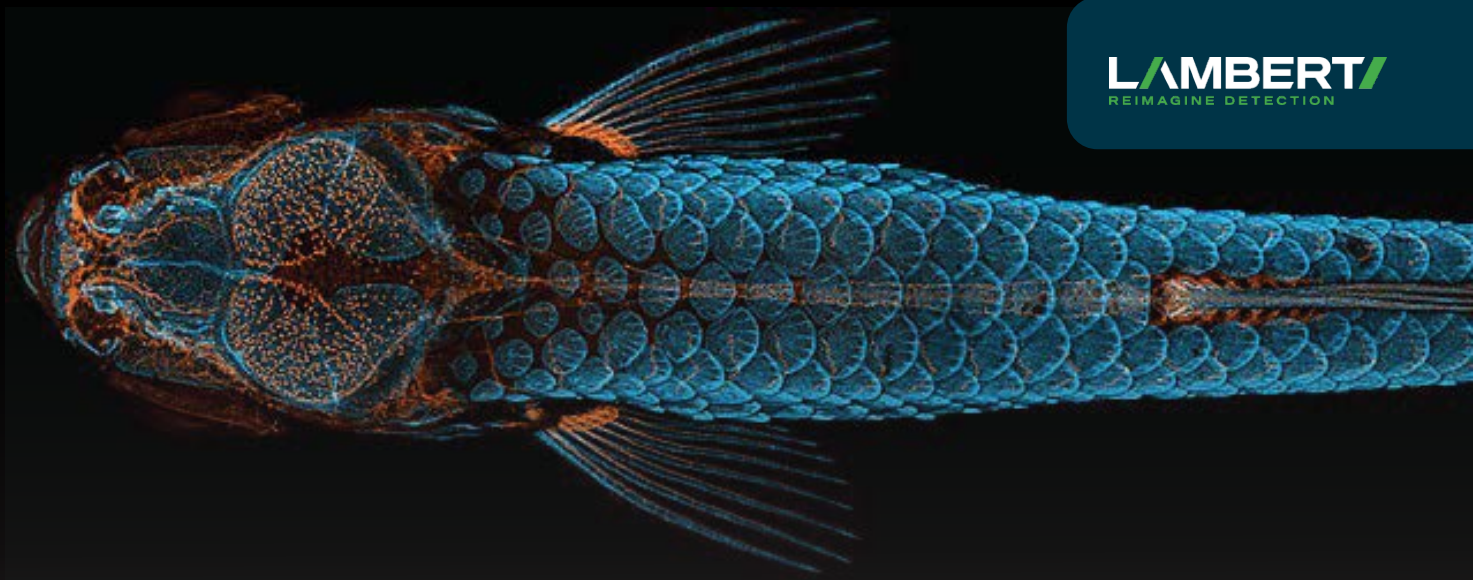
50 L

65 L

85 L

105 L

Application Showcase



LAMBERT
REIMAGINE DETECTION

High-speed *in vivo* imaging of a zebrafish heart

High-Resolution Imaging for the Next Generation Life Science Research using the Lambert HiCAM Fluo

Cellular imaging developments are essential for speeding up biological, pharmaceutical, and diagnostic discoveries. HiCAM, a cutting-edge high-resolution imaging platform, is revolutionising the way scientists quickly and clearly visualise, and measure intricate cellular processes. HiCAM provides accurate, repeatable insights into cell morphology, signalling pathways, and phenotypic responses by fusing high-resolution optics, quick image acquisition, and potent analysis algorithms. The fundamental features of HiCAM, its uses in high-throughput screening, and its effects on workflows in both academic and commercial labs are examined in this application.

Introduction

Recording images of living organisms at high frame rates with a fluorescence microscope is challenging. High-speed imaging requires a considerable light intensity, because at high frame rates the image sensor is exposed to light very briefly. During that short period of time, enough light needs to be captured to obtain a clear image. Normally, this is achieved by increasing the intensity of the illumination. Because the lighter bounces off the object, the more light reaches the camera. But when studying fluorescence or chemiluminescence, the object itself emits light and increasing the intensity of the emitted light is often not possible. In such a situation, the solution is to increase the intensity of the light that is detected by the camera.

Keywords or phrases: High-resolution microscopy, cellular imaging, phenotypic screening, live-cell imaging, image-based analysis

Application Showcase



Figure 1. Photo of a zebrafish. The heart is located inside the red square.

Imaging the Cardiovascular System of a Zebrafish

At the Max Planck Institute for Heart and Lung Research in Bad Nauheim (Germany), the cardiovascular system of the zebrafish is studied. The transparency of the zebrafish (figure 1) and its experimental advantages make it an ideal scale model of the human cardiovascular system.

To study the blood flow in a zebrafish, the red blood cells are labelled with the fluorescent protein DsRed. The intensity of the fluorescent light is limited by the finite number of fluorescent proteins attached to the red blood cells. Also, the direction in which the light is emitted is random, which further decreases the amount of light reaching the camera. A low light intensity is not necessarily problematic. Increasing the exposure time to capture sufficient light is a well-known method for imaging dim objects that are stationary. However, using the same method on a moving object results in blurred images.

When imaging a living zebrafish, its internals are moving. The heart rate of a zebrafish is approximately 175 bpm, or nearly 3 beats per second. To capture each phase of the heartbeat requires a high frame rate, because otherwise the images will be distorted by motion blur. This means the image sensor is being exposed to the dim fluorescent light very briefly. Increasing the amount of fluorescent light by increasing

the intensity of the excitation light is not an option, as this would harm the fish.



Figure 2. HiCAM attached to fluorescence microscope.

Experimental Setup

The zebrafish is studied with a fluorescence microscope with high-speed camera system mounted to it (Figure 2). The fish is fixated in a gel and illuminated from below. Fluorescent light from the DsRed protein is emitted from the red blood cells. This light is emitted in every direction, some of it traversing the optical path of the laser in the opposite direction. But instead of being reflected back towards the light source, the fluorescent light is directed towards a camera through a dichroic

Application Showcase

mirror. Any scattered excitation light is reflected by the dichroic mirror. An optical filter removes any background light and only transmits light at the wavelength emitted by fluorescence of the red blood cells.

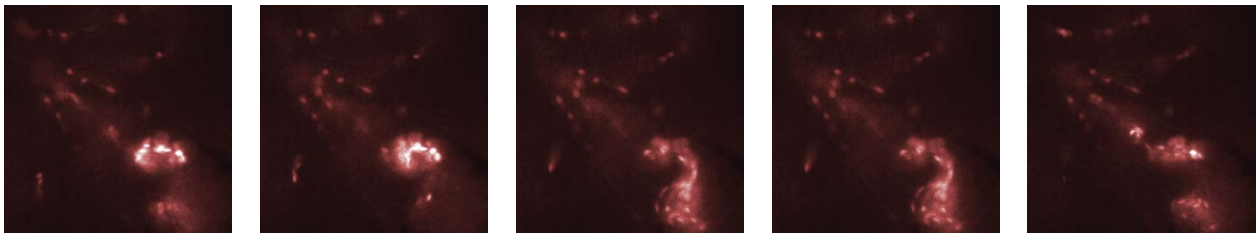


Figure 3. Red blood cells in the heart of a zebrafish (bottom right corner of images) are transported from one chamber to the next chamber (a-c) and into the aorta (e). Images shown here were recorded with an interval of 25 ms between them. Recording was done at 2000 fps with an exposure time of 500 us.

An image sensor will capture the incoming fluorescent light. At frame rates of hundreds or thousands of frames per second, the exposure time for each frame is in the order of several milliseconds to fractions of milliseconds. Electron-Multiplied CCD (EMCCD) sensors have a light sensitivity that is good enough to capture the dim fluorescent light. But they can only achieve frame rates up to approximately 100 fps at full resolution, which is not enough for the application at hand. CMOS sensors can operate at higher frame rates, up to thousands of frames per second at full resolution. However, during the short exposure time of each frame, a regular high-speed CMOS sensor is not able to record a sufficient amount of light to achieve a reasonable signal-to-noise ratio.

Advantages of the HiCAM

The HiCAM achieves both the required light sensitivity and the high frame rates by combining a high-speed CMOS sensor with an image intensifier. The image intensifier increases the number of detected photons by

several orders of magnitude. This way, it is possible to record the blood flow in a zebrafish at 2000 frames per second. Figure 3 shows the flow of red blood cells through the cardiovascular system of the zebrafish.



LAMBERT
REIMAGINE DETECTION

HiCAM Fluo

Cooled High-speed Camera for
Fluorescence Imaging

OD600®



Made in
Germany

Fast, easy, and accurate determination of cell density at 600 nm

Technical Specifications

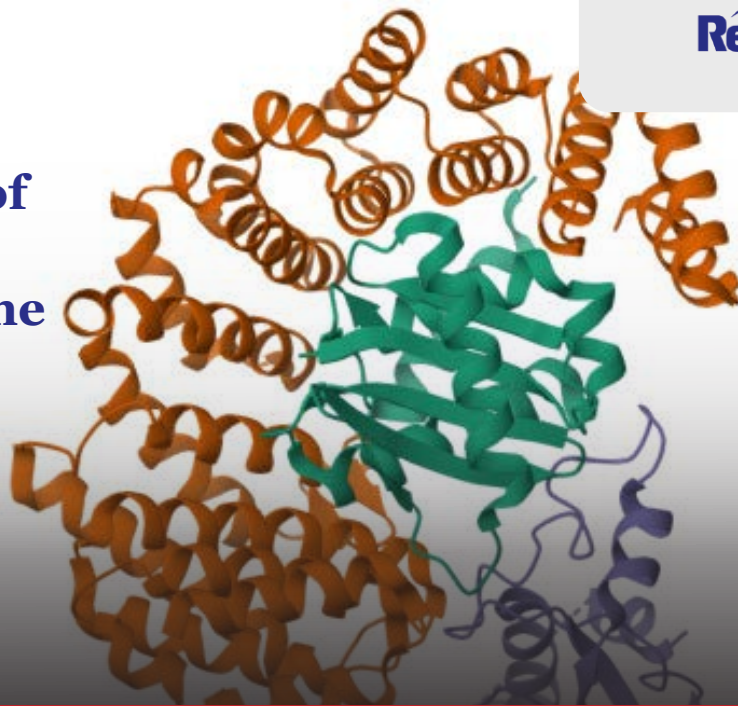
Wavelength	600 nm
Photometric Range	OD600: 0 – 4 A; McFarland: 0 – 16 MFU
Accuracy	OD600: @ 1A: < ±0.01 A McFarland: @ 0 – 8 MFU: ≤ ±0.1 MFU
Reproducibility	OD600: @ 1A: < ±0.002 A McFarland: @ 0 – 8 MFU: ≤ ±0.05 MFU
Cuvettes/Tubes	DiluCells; 10 mm macro- and semi-micro cuvettes; 10, 12, 16, 18 mm glass/falcon tubes – Without the need for adapters. Wipeable sample compartment – fixed with drain hole.

Well-Suited for Diverse Industries

- Microbiology and Biotechnology Research
- Protein Expression Studies
- Bioprocess Monitoring
- Quality Testing of Liquid Pharmaceuticals
- Water Quality Monitoring
- Breweries and Wineries
- Food and Beverage Industry
- Clinical and Medical Research
- Environmental Science and Industrial Applications

Application Showcase

SPR-Based Characterization of Binding Affinity and Residence Time for Potential Antiretroviral Compounds



Reichert
AMETEK

Using Reichert Surface Plasmon Resonance (SPR) for Screening of Small Molecule Inhibitors

The development of anti-retroviral agents depends on accurately identifying and characterizing molecular interactions with its target proteins.

In this application, the Reichert® 4SPR system enables a comprehensive label-free analysis of inhibitor analogues against HIV-1 Nef. The application also highlights the strategic advantage of SPR in translating medicinal chemistry efforts into clinically relevant candidates.

Introduction

Surface Plasmon Resonance (SPR) can be used as an effective tool for screening many samples against a target or targets immobilized on a sensor chip¹⁻³. Often researchers do initial research showing that a certain molecule with a particular molecular backbone can act as an inhibitor to a given protein. Then they follow up with analogues to see if efficacy can be improved by making structural changes to the original molecule including addition of other functional groups.

This application highlights use of SPR in the characterization of inhibitor analogues and determination of structure-activity relationships which ultimately could aid in the development of a new class of anti-retroviral drugs¹.

Keywords or phrases: Surface Plasmon Resonance, SPR, small molecule inhibitors, HIV-1 Nef, binding, screening, kinetics

Application Showcase

Background

Earlier research identified a small molecule inhibitor of HIV-1 Nef which was shown to block several of its activities related to enhancement of viral infectivity and replication¹. In the current research, 216 analogues of the original compound were synthesized and screened against recombinant Nef protein using SPR. The analogues all contained the same hydroxypyrazole scaffold from the original inhibitor (core molecule in the inset above) but with modifications at the A, B and C positions. From the SPR data obtained, compounds were compared based on affinity, extent of binding, and residence time (which is calculated from the reciprocal of the dissociation rate constant ($1/K_{off}$))¹.

Studying the SPR results, the top scoring inhibitors were found to share certain features, including a slow off rate. None of the top analogues returned to baseline over the course of a 3-minute dissociation, suggesting that these inhibitors might induce a change in the conformation of Nef that enables tight binding. However, no covalent bond was formed, since the analogues dissociated in weak base. Researchers at the University of Pittsburgh developed an “Activity Score” which combined multiple SPR parameters with anti-retroviral activity into a single numerical value for each analog providing an unbiased ranking of the compounds which helped them rank the analogues for further testing¹.

Experimental Conditions

- Instrument: Reichert® 4SPR
- Sensor Chip: Carboxymethyl Dextran
- Temperature: 25 °C
- Target: Recombinant, full-length HIV-1 Nef
- protein (NL4-3 allele)
- Analyte: Various
- Running Buffer: PBS + 1% DMSO
- Flow Rate: 50 µL/min
- Association Time: 1.5 minutes
- Dissociation Time: 3 minutes
- Regeneration: 5 mM NaOH for 30 seconds

Results

Forty-five of the analogues showed no binding. The remainder were ranked based on SPR kinetics, the size of the SPR response and their activity from a cell-based HIV-1 infectivity assay. Sensorgrams were fit to either a 1:1 model or a conformational change model. Affinities varied widely from low micromolar to picomolar. The top six analogues bound Nef with KD values ranging from about 0.65 pM (FC-7943) to 10 nM (FC-8698)¹.

Results for two of the top six compounds are shown here:

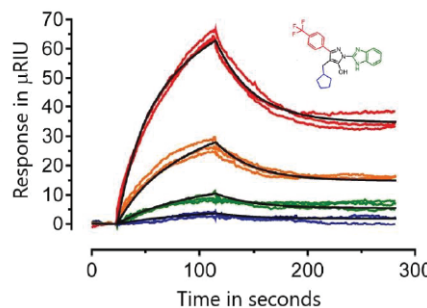


Figure 1: The SPR sensorgrams obtained for compound 7902 are shown fit to a 2-step model. Compound 7902 has the structure shown in the inset and shares, at the A-position, a phenyl group substituted at the para position by a hydrophobic trifluoromethyl group, with three of the other top compounds. The KD is 93.6 pM and the residence time is 3.79e5 minutes, with 96.1% infectivity inhibition at 1 µM. Each analog concentration was measured in triplicate (30 µM, red; 10 µM, orange; 1.1 µM, green; 1.1 µM, blue), with the fitted curves shown in black.

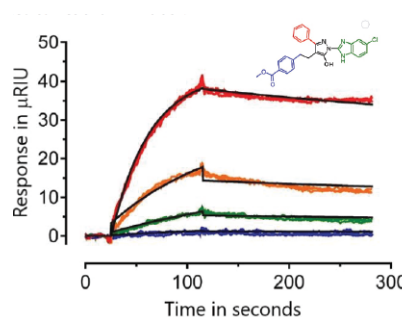


Figure 2: The SPR Sensorgrams obtained for compound 8698 are shown here, fit to a 1:1 model. Compound 8698 has the structure shown in the inset and shares a chloro-benzimidazole group at the C-position with one other of the top compounds. The KD is 13 nM, the residence time is 780 minutes, with 100% infectivity inhibition at 1 µM. Analogue concentrations as per the legend to Figure 1.

Application Showcase

Conclusion

The screening example outlined here highlights how useful it is to do *in vitro* testing in real time using SPR. For this example, several hundred inhibitors were tested and ranked based on their kinetics and activity. By using SPR to help create an “Activity Score”, researchers were able to determine the top compounds to take into further testing. Their structure–activity approach led these researchers to identify new analogues with high affinity for Nef that also show strong antiretroviral activity and maintain the ability to reverse down regulation by Nef of MHC-I at the cell surface¹.

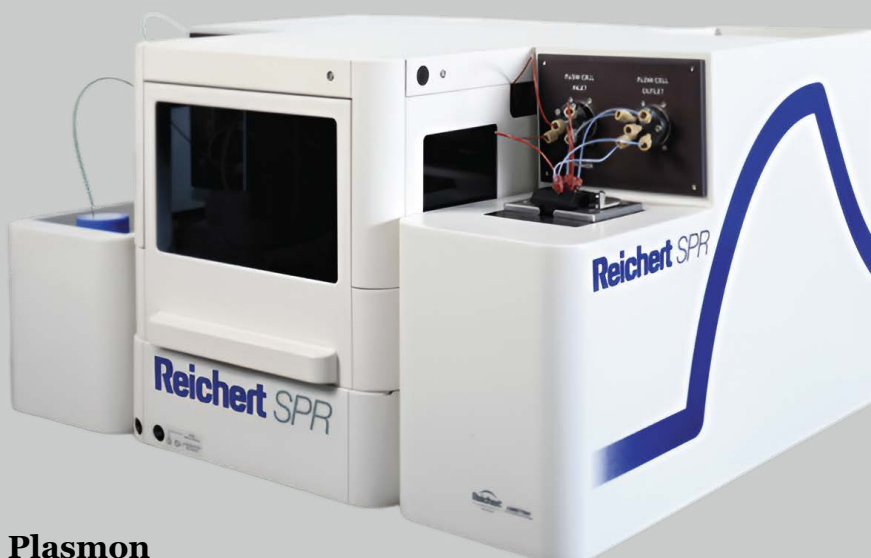
References

1. Shi, H.; Tice, C. M.; Emert-Sedlak, L.; Chen, L.; Li, W. F.; Carlsen, M.; Wrobel, J. E.; Reitz, A. B.; Smithgall, T. E. Tight-Binding Hydroxypyrazole HIV-1 Nef Inhibitors Suppress Viral Replication in Donor Mononuclear Cells and Reverse Nef-Mediated MHC-I Downregulation. *ACS Infectious Diseases* 2019, 6 (2), 302–312. <https://doi.org/10.1021/acsinfecdis.9b00382>.
2. Brengel, C.; Thomann, A.; Schifrin, A.; Allegretta, G.; Kamal, A. A. M.; Haupenthal, J.; Schnorr, I.; Cho, S. H.; Franzblau, S. G.; Empting, M.; Eberhard, J.; Hartmann, R. W. Biophysical Screening of a Focused Library for the Discovery of CYP121 Inhibitors as Novel Antimycobacterials. *ChemMedChem* 2017, 12 (19), 1616–1626. <https://doi.org/10.1002/cmdc.201700363>.
3. Bestgen, B.; Kufareva, I.; Seetoh, W.; Abell, C.; Hartmann, R. W.; Abagyan, R.; Le Borgne, M.; Filhol, O.; Cochet, C.; Lomberget, T.; Engel, M. 2-Amino-thiazole Derivatives as Selective Allosteric Modulators of the Protein Kinase CK2. 2. Structure-Based Optimization and Investigation of Effects Specific to the Allosteric Mode of Action. *Journal of Medicinal Chemistry* 2019, 62 (4), 1817–1836. <https://doi.org/10.1021/acs.jmedchem.8b01765>.
4. Reprinted (adapted) with permission from Shi H, Tice C M, Emert-Sedlak L, Chen L, Li W F, Carlsen M, Wrobel J E, Reitz A B, Smithgall T E. “Tight-Binding Hydroxypyrazole HIV-1 Nef Inhibitors Suppress Viral Replication in Donor Mononuclear Cells and Reverse Nef-Mediated MHC-I Downregulation”, ACS Infect Dis, 2020, 6, 302–312. doi:10.1021/acsinfecdis.9b00382. Copyright © 2019 American Chemical Society.



Reichert® 4SPR

4-Channel Surface Plasmon Resonance System



BIOSAFETY CABINET

Features:

- **Microprocessor Controller** with large LCD display for real-time monitoring of hepa filter status
- **EC Fan** achieving 30-60% energy savings compared to AC motors.
- **HEPA Filter** with a ISO class 5 cleanliness and >99.99% filtration efficiency at 0.3 μm .
- **Internal Working Area** with a special negative pressure design preventing contaminants from escaping into the operator's environment.
- **Ergonomic Design** with a 5° backward-slanted safety glass for comfortable viewing.



Triple Quadrupole Mass Spectrometry for the Quantification of Monoclonal Antibody Light Chains in Plasma

A Robust LC-MS/MS Method Utilizing the Waters Xevo TQ-XS Mass Spectrometer

Caitlin Dunning, Mary E. Lame, Mark D. Wrona
Waters Corporation

The work herein describes the development and optimization of sample preparation and LC-MS/MS methodology for the sensitive quantification of mAb subunit light chains using selective column chemistry and triple quadrupole mass spectrometry.

Keywords or phrases: Monoclonal, antibody, immunopurification, rat plasma, triple quadrupole mass spectrometry.

Introduction

The increasing complexity of biotherapeutics is driving the need for more informative, selective, sensitive quantitative methods and sample preparation techniques. Although surrogate peptide methodology remains popular and has become increasingly easier to deploy, more direct measurements of monoclonal antibodies or their subunits is increasingly desired¹. This is an area where high resolution mass spectrometers demonstrate utility largely due to their extended mass range and resolution capabilities, however there are many instances where it may be appropriate and possible to transfer these assays to triple quadrupole mass spectrometers².

Triple quadrupole instruments are ubiquitous in bioanalytical labs, robust, reliable, and suitable for large studies.

Application Showcase

Instruments with a mass range up to 2000 m/z can accommodate the identification and quantification of relatively large proteins including mAb subunit light chains (~23 kDa). An ongoing challenge in the analysis of larger molecules that must also be addressed is adequate chromatographic separation, especially at the low concentration levels required of many bioanalytical studies. The work herein describes the development and optimization of sample preparation and LC-MS/MS methodology for the sensitive quantification of mAb subunit light chains using selective column chemistry and triple quadrupole mass spectrometry. Extracted from 10 μ L of rat plasma, lower limits of quantification of 25 ng/mL of adalimumab subunit light chains were achieved.

Experimental

Sample preparation

Preparation of samples, calibration standards, and QC samples

Calibration curve standards and quality control (QC) samples of adalimumab were prepared in commercially available rat plasma at various concentration levels (25–100,000 ng/mL). All calibration curve standards and blanks were prepared in triplicate, and all QC levels were prepared in quintuplicate. With the exception of blanks, all samples were spiked with cetuximab as the internal standard (ISTD).

Immunopurification

Adalimumab and its ISTD were extracted from plasma with biotinylated goat anti-human Fc antibody coupled to streptavidin coated magnetic beads (Promega P/Ns V7830 and V7820). 25 μ L of bead slurry was aliquoted, washed, and equilibrated with tris buffered saline (TBS, 25 mM Tris, 150 mM NaCl, pH 7.2) prior to incubation with biotinylated antibody. 15 μ L of biotinylated antibody was diluted to 100 μ L with TBS and incubated for one hour with mixing (1200 rpm) at room temperature. Following incubation, beads were washed and equilibrated with TBS. 10 μ L of rat plasma samples,

10 μ L of ISTD, and 80 μ L of TBS were combined with the anti-human Fc antibody charged streptavidin beads. Samples were incubated with mixing (1200 rpm) for one hour at room temperature, washed two times with TBS, and then washed two times with water to remove salts. The immunopurified samples were eluted from the beads with a 0.1% formic acid solution (50 μ L), which was mixed for 15 min. Eluates were transferred to a clean PCR plate and then neutralized to pH 8.0 with 500 mM ammonium bicarbonate (5 μ L).

Reduction and Alkylation

Following affinity purification, samples were reduced and alkylated with reagents from the ProteinWorks AutoeXpress Reduction/Alkylation Kit. Dithiothreitol (DTT) and iodoacetamide (IAM) were prepared in 50 mM ammonium bicarbonate at ProteinWorks kits' stock concentrations of 70 mM and 142 mM respectively.

These stocks were then diluted further with 50 mM ammonium bicarbonate to 12 mM and 78 mM respectively immediately prior to addition to samples. Affinity purified samples (55 μ L) were reduced with 5 μ L DTT (final concentration 1 mM) for 20 minutes at 37 °C, then alkylated with 5 μ L of IAM (final concentration 6 mM) for 30 minutes at room temperature in the dark. Samples were acidified with 5 μ L of formic acid (final concentration 1% v/v) and injected (10 μ L) for LC-MS/MS analysis.

LC-MS/MS method conditions

Component	Details
LC System	ACQUITY UPLC I-Class PLUS (Fixed Loop)
Detection	Xevo TQ-XS Mass Spectrometer, ESI+
Column	BioResolve RP mAb Polyphenyl Column 450 Å, 2.7 μ m, 2.1 \times 50 mm
Column Temperature	80 °C
Sample Temperature	15 °C
Injection Volume	10 μ L

Application Showcase

Mobile Phase A	0.1% Formic acid in water
Mobile Phase B	0.1% Formic acid in acetonitrile
MS System	Xevo TQ-XS
Capillary	2.4 kV
Cone	60 V
Source Offset	30 V
Source Temperature	150 °C
Desolvation Temperature	600 °C
Cone Gas Flow	150 L/hr
Desolvation Gas Flow	1000 L/hr
Collision Gas Flow	0.15 mL/min
Nebulizer Gas Flow	7 bar

System calibration: Low resolution (FWHM 1.0 Da)

Data Management	MassLynx (v4.2)
Quantification Software	TargetLynx

LC gradient:

Time (min)	Flow Rate (mL/min)	%A	%B	Curve
Initial	0.3	85	15	6
1	0.3	85	15	6
1.5	0.3	75	25	6
4	0.3	70	30	6
5.5	0.3	10	90	6
6.5	0.3	10	90	6
7	0.3	85	15	6
8.5	0.3	85	15	6

Results and Discussion

Measurement of subunits presents several opportunities over intact quantification, including a decrease in the complexity of data analysis and quantification. However, there are inherent limits to this type of analysis including mass range and resolution which make it more difficult to measure heavy chain Fc/2 subunits which may be glycosylated, adding complexity to the mass spectra. Quantification of the light chain region is desirable because it contains the CDR, or variable region, which can be used to differentiate mAbs which have high sequence homology with each other or endogenous IgGs³. Measurement of the light chain enables quantification of larger portions of the mAb and negates the need to identify unique surrogate peptides. Due to their size, light chain quantification assays can be transferred to triple quadrupole mass spectrometers enabling robust and reproducible quantification for large bioanalytical studies.

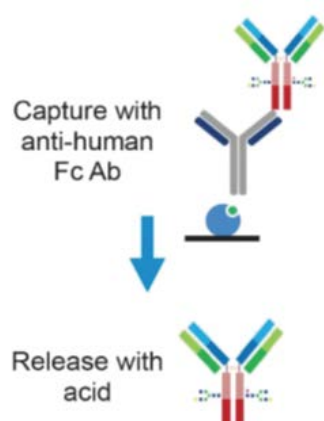
Sample preparation

Affinity purification combined with sample preparation for the mAb of interest is increasingly required for all LCMS assays in order to remove matrix interferences and achieve the highest levels of sensitivity. Adalimumab and its internal standard cetuximab were extracted from rat plasma using a selective affinity capture method (Figure 1.)⁴. Following immunopurification, a simple and fast sample preparation protocol was developed for the partial reduction of mAbs to their light and heavy chain subunit components. Partial reduction cleaves the light chains from the heavy chain at the hinge region and leaves internal disulfide bonds intact. During method development, stability studies (not shown) demonstrated that partially reduced light chains had stable signal over a large pH range (~1–10) when alkylated. In contrast, light chains were only stable under very low pH conditions, which may not be suitable for all types of analyses. To enable the use of this method under a variety of experimental conditions, alkylation was employed. The experiments described here seek to

Application Showcase

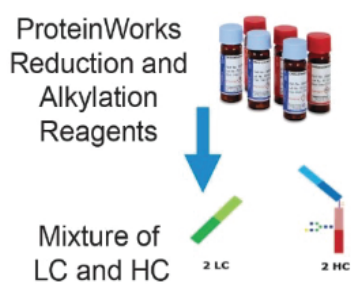
explore the feasibility of sensitive and rapid quantification of larger proteins via triple quadrupole mass spectrometry.

Immunopurification



- » Wash 25 μ L beads with 3 \times 200 μ L TBS Dilute 15 μ L anti-human Fc Ab with 85 μ L TBS
- » Incubate with beads 1 hour at RT
- » Wash beads with 2 \times 200 μ L TBS
- » Dilute 10 μ L plasma and 10 μ L ISTD with 80 μ L TBS
- » Incubate with beads 1 hour at RT
- » Wash beads with 2 \times 200 μ L TBS
- » Wash beads with 2 \times 200 μ L Water
- » Elute with 50 μ L 0.1% formic acid solution
- » Incubate 15 minutes at RT
- » Transfer to PCR plate, then neutralize with 5 μ L of 500 mM ammonium bicarbonate

Reduction And Alkylation



- » Reduce 55 μ L eluate with 5 μ L of 12 mM DTT
- » Incubate 20 minutes at 37 °C
- » Alkylate with 5 μ L of 78 mM IAM
- » Incubate 30 minutes at RT
- » Quench with 5 μ L of 14% formic acid (final conc. 1% v/v)

Figure 1. Sample preparation workflow for the quantification of adalimumab from rat plasma. Samples were immunopurified from 10 μ L rat plasma using biotinylated goat anti-human Fc antibody coupled to streptavidin coated magnetic beads. Immunopurification eluates were reduced to subunits with DTT, alkylated with IAM, and quenched with formic acid prior to LC-MS/MS analysis⁴.

Application Showcase

Chromatography

It is necessary to achieve complete chromatographic separation between the mAb of interest and its internal standard. This can be difficult to achieve with traditional columns and the short gradients desired for efficient bioanalytical analysis of potentially 100's of samples. Although full separation of these subunits can be achieved by increasing the length of the chromatographic gradient, we found that using alternative column chemistry can achieve the same goal. Shown in Figure 2, we were able to successfully separate adalimumab from its internal standard cetuximab using a BioResolve RP mAb Polyphenyl Column⁵ with a cycle time of only 8.5 min.

Furthermore, we demonstrate that BioResolve RP columns can be utilized for the sensitive quantification of mAb light chains with very little total protein on column (35.7 pg). Use of this column enabled a 2 \times reduction in total cycle time, and drastically improved light chain separation, enabling sensitive, fast, and reproducible quantification of adalimumab.

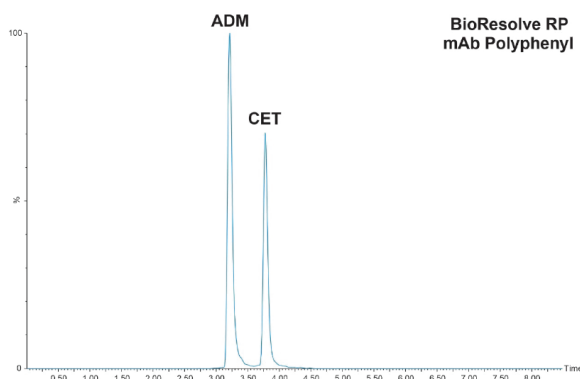


Figure 2. Representative chromatographic separation of mAb subunit light chains liberated from adalimumab and its internal standard cetuximab. Light chains were separated over a 2.5 min gradient using a BioResolve RP mAb Polyphenyl, 450 Å, 2.7 µm, 2.1 x 50 mm Column.

Mass Spectrometry

Characterization via Xevo G2-XS QToF

During assay development, adalimumab and cetuximab were well characterized via experiments performed on a

Xevo G2-XS QToF high resolution mass spectrometer. Figure 3, Panels A and B demonstrate that full scan spectra collected using a triple quadrupole and high-resolution mass spectrometer produce the same charge state envelopes, indicating that the most abundant precursors can be isolated and fragmented using either instrument. The Xevo G2-XS QToF Mass Spectrometer was used to discover and confirm selective product ions originating from the mAb subunit light chains and accurately determine the identity of these product ions (Figure 3, Panel C).

To aid in this, third party software ProSight Lite (Northwestern University)⁶ and Protein Prospector MS-Product function (UCSF)⁷ were leveraged to: identify light chain precursor ions, survey MS/MS scans to find selective b and y ions originating from the light chains and confirm the cleavage sites of these fragments. During this phase of method development, a sensitive product ion of the +18 and +19 precursors was identified at 1329.85 m/z, corresponding to the y-ion cleavage between Phe-118 and Pro-119 (Figure 4, Panel A). The region in which this cleavage occurs corresponds to a portion of the light chain sequence, which is conserved across many humanized IgG biotherapeutics, including adalimumab and cetuximab (Figure 4, Panel B). For this reason, this intense product ion is shared between the two mAbs and can be used for the quantification of both. A secondary, selective product ion corresponding to the b-ion cleavage of Val-115 and Phe-116 was identified at 1554.39 and 1556.24 m/z for adalimumab and cetuximab respectively. These product ions were used as qualifiers.

Application Showcase

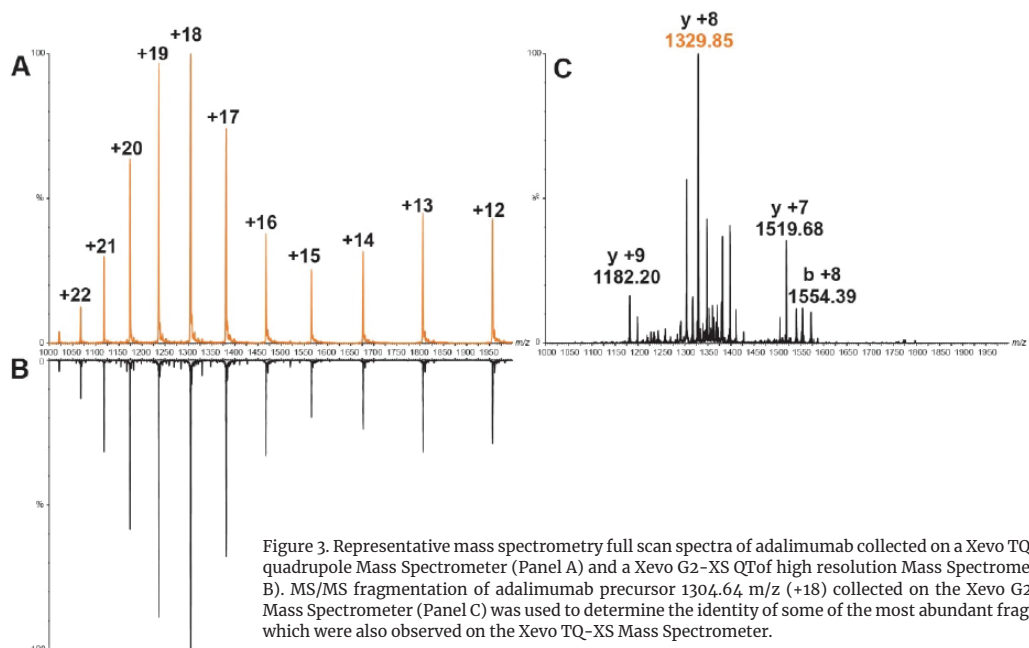


Figure 3. Representative mass spectrometry full scan spectra of adalimumab collected on a Xevo TQ-XS triple quadrupole Mass Spectrometer (Panel A) and a Xevo G2-XS QTOF high resolution Mass Spectrometer (Panel B). MS/MS fragmentation of adalimumab precursor 1304.64 m/z (+18) collected on the Xevo G2-XS QTOF Mass Spectrometer (Panel C) was used to determine the identity of some of the most abundant fragment ions which were also observed on the Xevo TQ-XS Mass Spectrometer.

A
FRAGMENT IDENTIFICATION AND MS PARAMETERS

Biotherapeutic	Precursor (m/z)	Fragment (m/z)	Cone (V)	Collision energy (eV)	Fragment identity
Adalimumab	1236.02 [+19]	1329.85 [+8]	60	27	P119 – y96
	1304.64 [+18]	1554.39 [+8]	60	32	V115 – b115
Cetuximab (ISTD)	1236.81 [+19]	1329.85 [+8]	60	27	P119 – y96
	1305.46 [+18]	1556.24 [+8]	60	27	V115 – b115

B
ADALIMUMAB LIGHT CHAIN SEQUENCE:

DIQMTQSPSSLSASVGDRVTITCRASQGIRNYLA
WYQQKPGKAPKLLIYAASTLQSGVPSRSGSGS
GTDFTLTISLQPEDVATYYCQRYNRAPYTFGQG
TKVEIKRTVAAPSVFIF |PPSDEQLKSGTASVCLL
NNFYPREAKVQWKVDNALQSGNSQESVTEQDSK
DSTYSLSSTTLSKADYEKHKVYACEVTHQGLSS
PVTKSFnRGEc

Figure 4. Fragment identification and MS parameters for adalimumab and cetuximab MRM transitions (Panel A). A common MS/MS fragment (1329.85 m/z, P119–y96) was identified from the conserved region of the adalimumab and cetuximab light chains, represented in Panel B^a.

Quantification via Xevo TQ-XS

This assay was then transferred to the Xevo TQ-XS, a triple quadrupole mass spectrometer. Full scan MS (Figure 3, Panel A) and MS/MS experiments (not shown) were performed on this instrument to confirm that the most abundant precursor and fragment ions were the

same on the high resolution and triple quadrupole mass spectrometers. Once confirmed, cone voltages and collision energies for the MRM transitions were optimized for the Xevo TQ-XS system (Figure 4, Panel A). To further improve sensitivity, the system was calibrated at low resolution, 1.0 Da at FWHM for both

Application Showcase

quadrupoles (in contrast to the standard ‘unit’ resolution of 0.75 Da at FWHM). This change in resolution settings improved assay sensitivity ~1.5 x with no significant changes to MS and MS/MS spectra quality. The Xevo TQ-XS System enabled fast, robust, and reproducible quantification of adalimumab light chains while maintaining the ease of use of triple quadrupole mass spectrometers.

Linearity, Precision and Accuracy

Sample preparation, LC, and MS methods were developed and optimized to enable linear, precise, and accurate quantification of adalimumab. Extracted from 10 μ L of rat plasma, lower limits of quantification (LLOQs) of 25 ng/mL were achieved. Calibration curves were linear ($r^2 > 0.99$) from 25–100,000 ng/mL using a $1/x^2$ fit (Table 1) and accurate within $\pm 15\%$, as well as QCs which achieved CVs <7%. QC performance is highlighted in Table 2 and chromatographic performance at the LLOQ is demonstrated in Figure 5.

Calibration Curve Statistics				
Curve (ng/mL)	Weighting	Linear Fit (R^2)	% Accuracy	LLOQ amount on column (pg)
25–1,00,000	$1/X^2$	0.993	87.0–18.9	35.7

Table 1. Linear dynamic range and standard curve statistics for adalimumab light chains extracted from rat plasma.

QC Statistics				
QC Level	QC Conc.	Mean (N=5)	Mean (N=5)	%RSD
		Calculated QC Conc.	% Accuracy	
LLOQ	25	24.4	97.4	6.1
LQC	75	74.7	99.6	2.9
MQC	2500	2798.3	111.9	2.5
HQC	80000	71386.7	89.2	1.9

Table 2. QC quantitative performance for adalimumab light chains extracted from rat plasma.

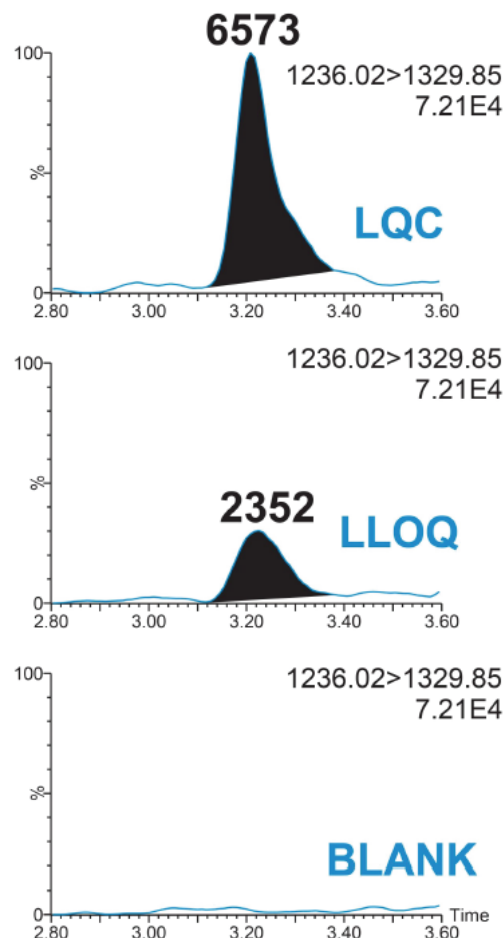


Figure 5. Representative blank, LLOQ, and LQC chromatograms for adalimumab light chains extracted from rat plasma.

Conclusion

Current biotherapeutics are both complex in structure and typically have high sequence homology to endogenous proteins and antibodies. Due to this, there may be very few peptides which are completely unique to a particular monoclonal antibody, such as adalimumab. Therefore, many peptides may suffer from matrix interferences which can hinder the lower limits of quantification. This provides an opportunity for proteins to be quantified at the intact or subunit level in order to avoid issues arising from the surrogate peptide method of analysis and the complex workflows associated with it. The work described here employs selective and specific sample preparation workflows and

Application Showcase

superior chromatographic separation of mAb subunit light chains. Combined with the identification of generic and sensitive MS/MS fragments, these methods enabled the high sensitivity, and accurate quantification of mAb subunit light chains via triple quadrupole mass spectrometry.

- » Highly specific immunoaffinity capture techniques and a simple workflow for the partial reduction of monoclonal antibodies were developed and optimized
- » BioResolve RP mAb Polyphenyl columns successfully resolved and enabled fast (8.5-minute cycle time) chromatographic separation of the mAb subunit light chains for both adalimumab and cetuximab
- » Using only 10 μ L of rat plasma, adalimumab subunit light chains can be quantified reliably, achieving LLOQs of 25 ng/mL and a linear dynamic range >3.5 orders of magnitude.

References

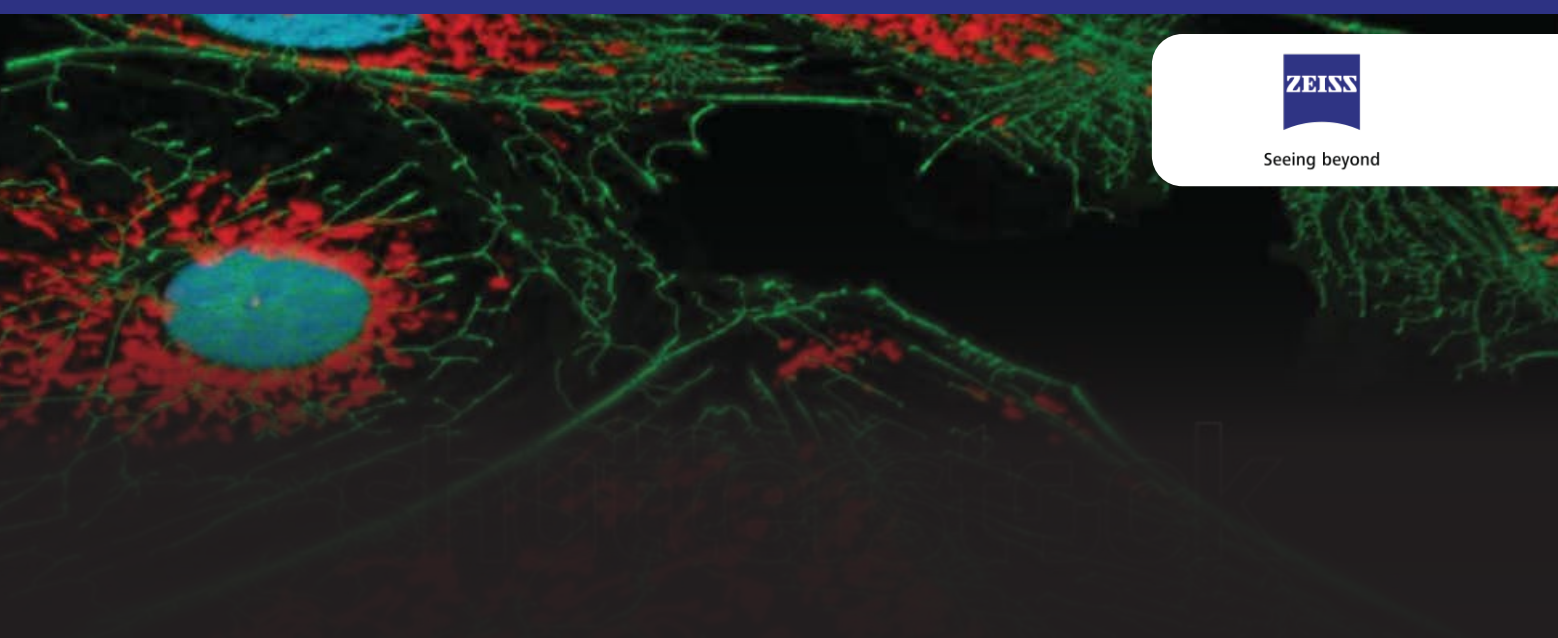
1. Ladwig, P.M.; Barnidge, D.R.; Willrich, M.A.V.; Mass Spectrometry Approaches for Identification and Quantitation of Therapeutic Monoclonal Antibodies in the Clinical Laboratory. *Clinical and Vaccine Immunology (CVI)*. 24:5 (2017): e00545–16.
2. Wang, E.H.; Combe, P.C.; Schug, K.A.; Multiple Reaction Monitoring for Direct Quantitation of Intact Proteins Using a Triple Quadrupole Mass Spectrometer. *J. Am. Soc. Mass Spectrom.* 27 (2016): 886–896.
3. Mills, J.R.; Corne, D.; Dasari, S.; Ladwig, P.M.; Hummel, A.M.; Cheu, M.; Murray, D.L.; Willrich, M.A.; Snyder, M.R.; Hoffman, G.S.; Kallenberg, C.G.M.; Langford, C.A.; Merkel, P.A.; Monach, P.A.; Seo, P.; Spiera R.F.; St. Clair, E.W.; Stone, J.H.; Specks, U.; Barnidge, D.R.; Using Mass Spectrometry to Quantify Rituximab and Perform Individualized Immunoglobulin Phenotyping in ANCA-Associated Vasculitis. *Analytical Chemistry*. 88 (2016): 6317–6325.
4. Dunning, C.M.; Lame, M.; Wrona, M.; Haynes, K.; Tackling Non-Specific Binding of Biotherapeutics Using LCMS Compatible QuanRecovery Sample Plates with MaxPeak High Performance Surfaces. *Waters Application Note* 720006528EN, March 2019.
5. Nguyen, J.M.; Kizekai, L.; Walsh, D.; Cook, J.; Lauber, M.A.; A Novel Phenyl Bonded Phase for Improved Reversed-Phase Separations of Proteins. *Waters Application Note* 720006169EN, January 2018.
6. Fellers, R.T.; Greer, J.B.; Early, B.P.; Yu, X.; LeDuc, R.D.; Kelleher, N.L.; Thomas, P.M.; ProSight Lite: Graphical Software to Analyze Top-Down Mass Spectrometry Data. *Proteomics*. 15:7 (2015): 1235–1238. Accessed July 2018 from <http://prosightlite.northwestern.edu/>.
7. Protein Prospector, “Proteomics Tools for Mining Sequence Databases in Conjunction with Mass Spectrometry Experiments.” Accessed July 2018, v. 5.22.1, at <http://prospector.ucsf.edu/prospector/mshome.htm>.
8. Adalimumab, protein sequence. Retrieved 15 Aug 2018 from <https://www.drugbank.ca/drugs/DB00051>.

Waters™
THE SCIENCE OF WHAT'S POSSIBLE.™



**Xevo TQ-XS
Triple Quadrupole
Mass Spectrometer**

Application Showcase



3D Fluorescence Imaging with Structured Illumination

Optical Sectioning in Widefield Fluorescence Microscopy with ZEISS Apotome

Dr. Soren Prag
Carl Zeiss Microscopy GmbH, Germany

3-dimensional fluorescence often produces images with less clarity due to out-of-focus light, particularly in thick specimens. Structured Illumination Microscopy (SIM) provides an effective optical sectioning method that enhances image contrast and resolution by eliminating the unwanted background fluorescence. This application explores the principles, optimisation strategies and advantages of ZEISS Apotome imaging, providing practical insights into grid selection, phase acquisition and the benefits of combining SIM with deconvolution for advanced biological imaging.

Keywords or phrases: Structured Illumination Microscopy (SIM), optical sectioning, 3D fluorescence imaging, grid, contrast, deconvolution, widefield microscopy

Introduction

In conventional widefield fluorescence microscopy an image contains light collected from the structures in the plane of focus as well as light from structures above and below this plane. The light from structures above and below becomes visible in the focal plane because of diffraction and interference and creates a blur in the image.

Diffraction and interference are physical phenomena where light waves interact with each other causing a blurring of the object of interest.

Consequently, a point object which is smaller than the resolution limit of the objective when imaged in 3D is not imaged as a point but as an hourglass shape known as Point Spread Function (PSF). When studying thick specimen, this out-of-focus light degrades the image quality by increasing the background fluorescence in the

Application Showcase

image and therefore decrease the signal-to-noise ratio (SNR) and the image contrast.

Such images are often not suitable for reasonable analysis and interpretation of the 3-dimensional structure of the objects.

Therefore, the motivation is to remove the out-of-focus light and obtain images of the objects of interest with highest contrast and highest resolution. This is the principle in optical sectioning. Besides the predominant confocal method using a pinhole in an optically conjugate plane, other approaches have been developed to obtain optical sectioning, including Structured Illumination.

As mentioned above, the main motivation of optical sectioning is improving the contrast by removing the out-of-focus light. This usually comes at the expense of decreasing the overall signal. When imaging weakly fluorescing samples this can be overcome by increasing the thickness of the optical section or by increasing the acquisition time. The latter has the negative side effect of putting higher burden on the sample leading to bleaching and increased phototoxicity, whereas the former increase the SNR. So, the major trade-off when doing optical imaging is the decrease in signal, and the skill of the operator to define the compromise between signal, resolution (i.e. thickness), photodamage and acquisition time. The thickness of the optical section is determined differently dependent on the sectioning method applied.

For instance, in confocal scanning microscopy, the size of the pinhole determines the thickness of the optical section. Increasing the pinhole will increase the thickness of the optical sample and increase the overall signal. The optimal thickness of the optical section is also determined by the numerical aperture (NA) of the objective lens, where high NA allows for thinner optical sectioning. In structured illumination, the thickness of the optical section can be altered by changing the frequency of the grid pattern. This also means that different objectives lenses with various numerical

apertures require different grid pattern frequencies.

The principle in structured illumination used in Apotome, is based on projection of a defined grid into the focal plane of a widefield fluorescence microscope. As the grid is moving in a lateral manner, a defined number of images, termed phases, are captured by a camera. The light emitted by structures, which are in the focal plane, will vary strongly in intensities when the illuminating grid lines move across them. If structures are not in focus, the wandering grid lines will not cause the emitted light to fluctuate as strongly.

By calculating the difference between the different phase images, it is possible to discriminate between in-focus and out-of-focus light. The differences in intensities are calculated pixel-by-pixel and the final image contains only the in-focus information which is an optical section.

Optimal Choice of Grid Pattern

Apotome is equipped with a motorized grid changer, which allows to select between three grid patterns: Low, Medium, and High (Figure 1).

The grid patterns in Apotome are different for Axio Imager.2, Axio Observer, and Axio Zoom.V16, which is due to differences in the optical path between the three stands. The grid pattern determine the thickness of the optical section (box 1).

This application focuses on Axio Observer, but the principles are the same for all stands.

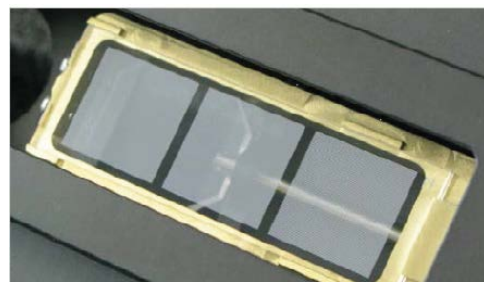


Figure 1: Three grid patterns available in ZEISS Apotome. The change between the pattern is controlled by the software (or the user) and is optimized according to the selected objective.

Application Showcase

Fluorescence image stacks of a 1 μm green, fluorescent beads on Axio Observer were acquired using the three grid patterns.

As shown in figure 2, the different grid patterns decreases the size of the point spread function (PSF) independently of the objective. As shown in the top panel for the Plan- APOCHROMAT 20x / 0.8 objective (compare Figure 2, a – d), the axial expansion of the PSF is clearly reduced when changing the grid pattern. Figure 2a shows the XZ plane of the PSF when observed in widefield microscope, figures 2b-2d show the axial expansion for the High, Medium, and Low grid pattern respectively.

Also, the PSF size observed using a Plan-APOCHROMAT objective 40x / 1.4 is reduced in combination with Apotome (Figure 2, lower panel).

When comparing the PSF acquired using widefield and high grid, a significant reduction is observed (compare Figure 2; a' and b') but in contrast to the Plan- APOCHROMAT objective 20x / 0.8, the PSF of Plan-APOCHROMAT 40x / 1.4 is only reduced minimally when changing the grid pattern from Medium to Low (compare Figures 2, c' and d').

This demonstrates the rationale for the automatic grid pattern selected by the software and highlights the importance of the different grid patterns. The optimal choice of grid pattern is achieved, when the diffracted light above and below the core of the PSF is effectively removed but without making the optical section too thin. This would result in an increase in signal-to-background, which in return would reduce the contrast. As shown, the low grid pattern is the optimal choice for Plan-APOCHROMAT 20x / 0.8, whereas for Plan-APOCHROMAT 40x / 1.4 the Medium grid pattern is the optimal choice. As a rule of thumb, the high magnification and / or high numerical aperture require High / Medium grid patterns, and low magnification and / or low numerical aperture require Medium / Low grid patterns.

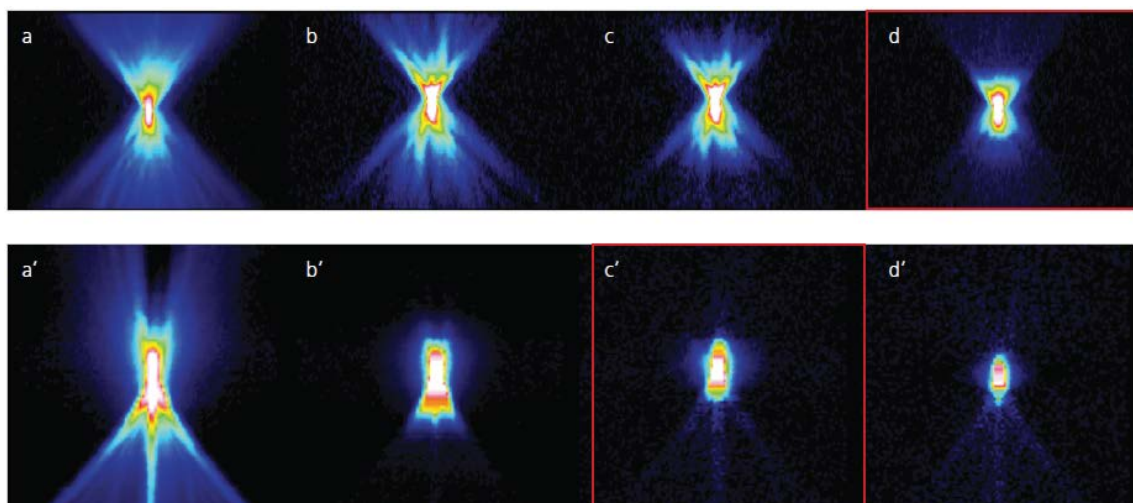


Figure 2: PSF of 1 μm bead using Plan-APOCHROMAT 20x / 0.80 (top panel) and Plan-APOCHROMAT 40x / 1.4 Oil. The XZ view is shown for widefield (a), High (b), Medium (c), and Low (d) grid patterns were used for acquisition. The red box highlights the automatic choice of grid pattern.

Application Showcase

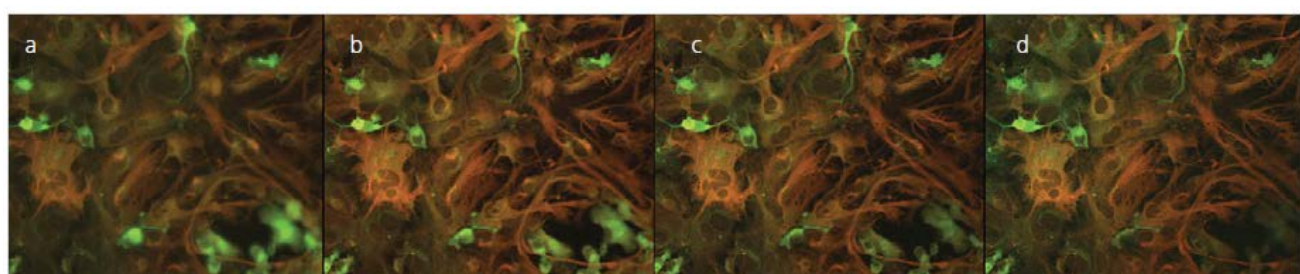


Figure 3a: Grid pattern determines the thickness of the optical section. α -Cathepsin B:Alexa 488 and α -GFAP:Alexa546 staining of astrocytes imaged using Plan-APOCHROMAT 40x / 1.4 Oil with widefield (a) Low (b), Medium (c) and High (d) grid pattern.

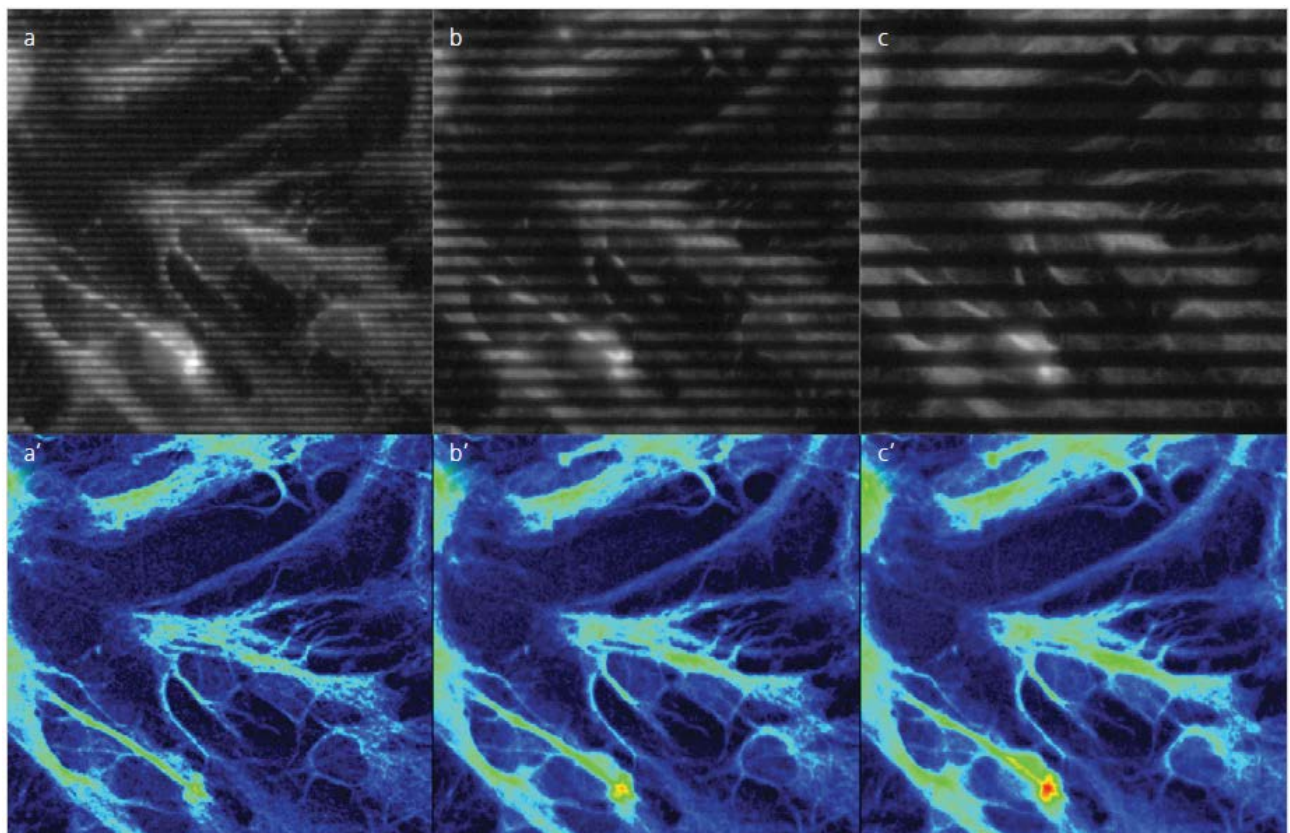


Figure 3b: Grid pattern determines the thickness of the optical section. GFAP:Alexa545 staining of astrocytes imaged using Plan-APOCHROMAT 40x / 1.4 Oil with Low (a, a'), Medium (b, b') and High (c, c') grid pattern. In upper panel (a – c) the raw images with the projected grid pattern are shown. The upper row shows raw images with grid lines, the lower row shows corresponding optical sections with identical settings for the look up table (LUT). The lower images show the optical sections derived from.

Thus, the grid pattern alters the PSF, which consequently determines the thickness of the optical section. This flexibility can be used beneficially by the user to increase the signal in weak fluorescent samples by giving up some resolution or increase the contrast in bright samples by deliberately choosing a lower or

higher grid pattern respectively.

As shown in figure 3, using the grid pattern increases the signal-to-background compared to the widefield settings (compare 3a – widefield and 3b – Apotome). Moreover, when changing the grid pattern from

Application Showcase

Medium to Low (compare figure 3c and 3d), the contrast is noticeably enhanced, and the section becomes thinner. This become more obvious when viewing a single channel only (compare Fig. 3a' – d').

The Number of Phases

The grid is shifted by a given number of phases in such fashion that all in-focus structures in the sample become covered once by the moving grid line. Each phase image is captured as an individual image prominently showing the grid lines.

The resulting CZI image contains all phase images and is called Apotome raw image. The optical section is then processed from the raw images online when viewing the

image in the ZEN imaging software. The number of phases / images can be selected in ZEN and varies from 3 to 15 with 5 phases being the default. The number of phases has little to no effect on the size of the PSF but has a marked influence on the quality of the processed image. As shown in figure 4, the XZ view PSF of a 1 μm bead is unaltered from images captured using 3 (a), 5 (b) and 10 (c) phases. However, as structured illumination is based on subtraction of consecutive images, this technique is sensitive to bleaching and vibration especially when occurring during capture of individual phase images. This has been addressed in the ZEN imaging software with advanced correction algorithms for bleaching and minor off-grid positions. These corrections remove any residual grid lines effectively. In extreme cases images can still be salvaged by employing an additional Fourier filter which stamps out grid lines.

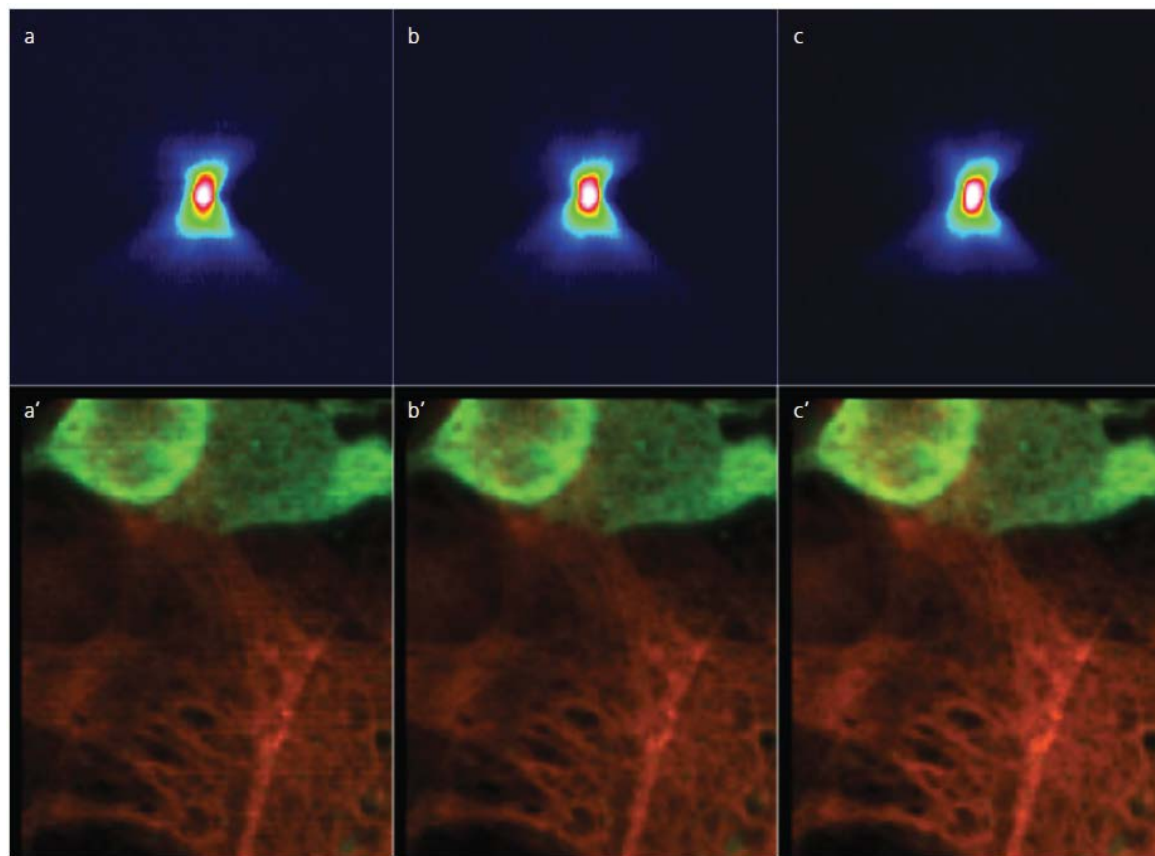


Figure 4: Number of phases determines the signal-to-background and has no impact on the PSF. XZ view of a 1 μm bead (a – c) and close-up detail of astrocytes stained with α -Cathepsin B:Alexa 488 and α -FAP:Alexa546 (a' – c'). The images were captured using 3 phases (a, a'), 5 phases (b, b'), and 10 phases (c, c'), and captured using Plan-APOCHROMAT 40x/1.4 Oil.

Application Showcase

An increase in the number of phases is a good practice for three reasons: first, it serves to decrease camera noise due to averaging. Secondly, it minimizes the occurrence of residual stripes in the processed image. Thirdly, and probably most importantly, an increase in the number of phase images can increase the resolution when combined with Deconvolution.

images processed from 5 (b') and 10 phases (c'). Furthermore, the signal-to-background ratio is improved with the number of phases (compare c' to b' / a') due to added benefit of averaging.

Apotome raw images can be subjected to a regularized inverse filter 3D-deconvolution.

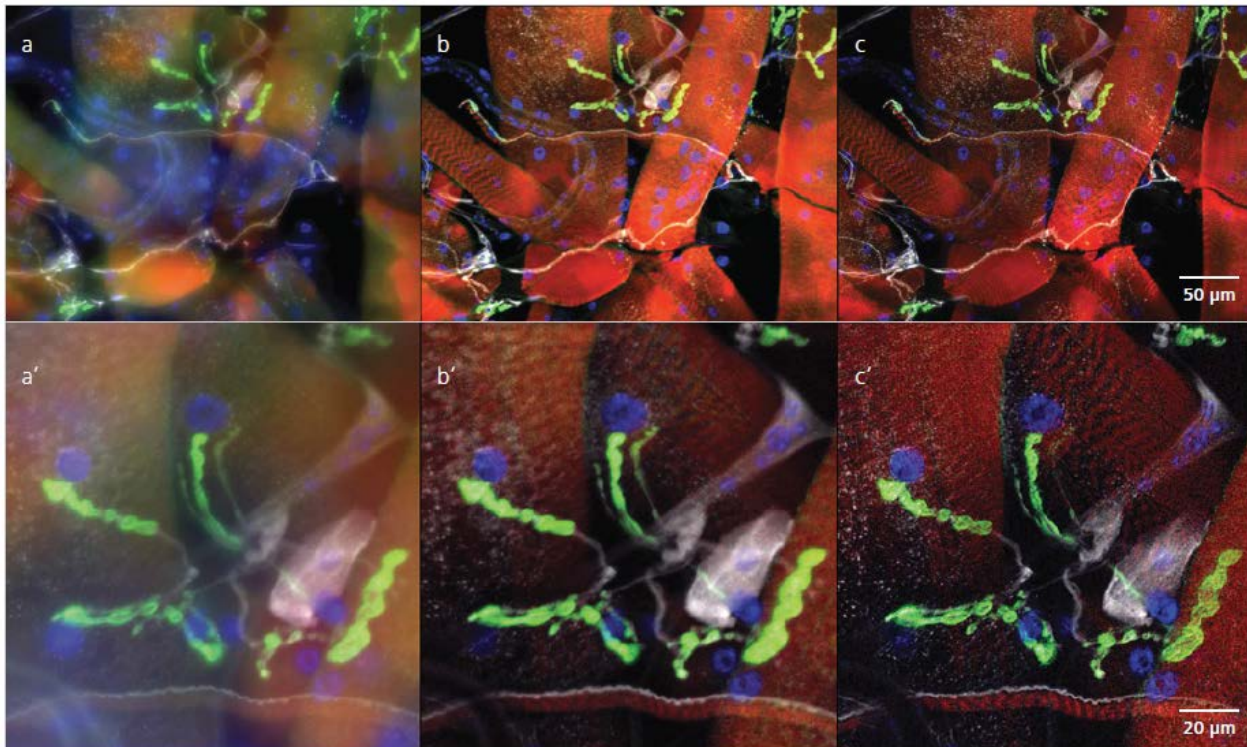


Figure 5: Deconvolution in combination with Apotome improves spatial resolution and restores information. *Drosophila melanogaster* neuromuscular junctions, acquired with Plan-NEOFLUAR 40x/0.75 objective. 6 phases were acquired. Green (Alexa 488): synapses, Red (Alexa 568): muscle; White (Alexa 647): motor neurons; Blue (Hoechst 33258): nucleus. Courtesy of K. V. Raghavan, National Centre for Biological Sciences, Bangalore, Republic of India. Shown in the upper panel is a maximum intensity projection of the z-stack processed as widefield (a), sectioned (b) and sectioned/deconvolved (c), scalebar shows 50 μ m. The lower panel shows a larger magnification of a single neuromuscular junction in widefield (a'), sectioned (b') and sectioned/deconvolved (c') processing, scalebar shows 20 μ m.

ZEISS Apotome and Deconvolution

The decision to preserve the phase images when capturing images using Apotome has an important consequence:

As shown in figure 4 (lower panel) the number of phases improves the signal and minimizes residual stripes:

processing images from 3 phases only, residual stripes are quite apparent in the image (a') when compared to

While 3D-deconvolution can in principle be applied to all fluorescence images, either widefield or confocal, if you have knowledge about the PSF of the acquisition conditions, the combination of structured illumination and deconvolution provides some unique advantages to classical deconvolution. In widefield deconvolution the PSF is fairly large and in order to reconstruct 3D information, iterative processing steps have to be employed to achieve at least a partially confocal PSF.

Application Showcase

The major advantage of this is, that all light emanating from the sample is being used making widefield deconvolution a very sensitive method for 3D imaging. In confocal microscopy, due to the optical sectioning capability of the microscope, 3D information is inherently captured at the expense of throwing away information which has been generated by the sample. Deconvolving confocal datasets can improve contrast and remove noise but can never restore the information lost during image capture.

Apotome deconvolution can do both: keeping the widefield information but at the same time creating optical sections via structured illumination. Signal is therefore restored based on the deconvolved widefield information and when combined with the optical sectioning properties of Apotome can lead to higher resolution results than either method alone could.

Figure 5 shows images of a drosophila neuromuscular junction section acquired with Apotome.2. Structures in the widefield image (a, a') are severely blurred and hard to see.

Adding standard Apotome processing already clears up the blur and reveals the structures (b, b'). However, the finer structures of the synapses e.g. only become visible in the deconvolved version of the image (c, c').

Due to the already confocal nature of the structured illumination, it is not necessary to employ iterative deconvolution algorithms. The rapid processing possible with the regularized inverse filter deconvolution provides best results while only adding moderate processing times making this combination even more attractive.

Conclusion

Optical sectioning using Apotome with ZEN provides features that were previously not well explained, particularly the variable grid pattern, phases, correction algorithms and the combination with 3D-deconvolution.

The choice of grid pattern determines the thickness of the optical section. The user can take advantage of the different grid pattern for instance in order to increase the signal for samples with low signal (thick sectioning) or increase the signal-to-background (thin sectioning). The optimal grid pattern is determined by the software and is dependent on the objective and the excitation wavelength.

The number of phases increase the signal-to-background by a process similar to averaging of the images. Averaging reduces the random shot noise in the final image by calculating an average of each pixel from multiple images. As shown here, the number of phases do little to nothing against the thickness of the optical section. The optimal choice of the number of phases is a compromise between acquisition time and the expected signal-to-background in the final image.

When acquiring few phases (< 5), the processed images are prone to stripe artefacts. Acquiring significantly more phases than 5 will bleach the sample more at proportionally less benefit for image quality. Zeiss' recommendation is to use the default 5 phase setting as the low number of images causes little bleaching damage to the sample and the acquisition time is reasonable.

Deconvolution can increase resolution and restore the lower dynamic range of images after Apotome processing.

In Apotome processing the out-of-focus light is subtracted from the image containing both the focus and the out-of-focus light. This generates a final image with low signal.

Deconvolution increases the signal in the final image due to reassigning the out-of-focus to the focus plane and can enhance the resolution beyond the resolution limit.

Application Showcase

Materials List and Image Acquisition

1) Samples:

- a. 1 μm green / yellow fluorescent beads
- b. Astrocytes stained with α -GFAP (Alexa 546), and α -Cathepsin B (Alexa 488)

2) Stand: Axio Observer.Z1 configured for standard fluorescence microscopy

3) Light source: HXP 120

4) Filters:

- a) FS38 (Alexa 488 and green, fluorescent beads)
- b) FS43 (Alexa 546).

5) Objectives:

- a) Plan-APOCHROMAT 20x / 0.8
- b) Plan-APOCHROMAT 40x / 1.4 Oil

6) Channels were configured according to Smart Setup

7) 20 – 30 μm z-stacks were acquired using optimal settings

8) Neuromuscular junctions' section, NCBS Bangalore, India



ZEISS Apotome

Section Thickness

The section thickness is specified by the grid pattern.

$$\text{section thickness} = \frac{3.83}{16\pi} \times \frac{\lambda \times 10^{-3}}{n \times \sin^2(a/2) \times v \times (1-v/2)}$$

$$v = \frac{M \times \lambda \times f \times 10^6}{m \times NA}$$

M = objective magnification

n = refractive index of the immersion media

m = correction factor for stand

(1.3 for Axio Imager and 2.57 for Axio Observer)

λ = wavelength in nm

f = grid constant in lines per mm

As shown from the formula, the thickness of the optical section is determined by the objective in use (i.e. magnification, numerical aperture, immersion media), the excitation wavelength, the microscope stand, and the grid.

The ZEN imaging software will automatically calculate the theoretical section thickness based on the configuration in use, and the value is shown in the software. The automatic grid selection aims to keep the section thickness in proximity to one Rayleigh Unit, d :

$$d = \frac{2 \times \lambda \times n}{(NA)^2}$$

Example: Axio Observer equipped with Plan-APO-CHROMAT 20x / 0.8 has a calculated Rayleigh Unit and section thickness as follows. The automatic grid selection is indicated in bold.

High grid = 3.2 RU / 4.9 μm , Medium grid = 1.8 RU / 2.8 μm , and **Low grid = 1.0 RU / 1.5 μm** .

Axio Observer equipped with Plan-APOCHROMAT 40x / 1.4 Oil has a calculated section thickness as follows:

High grid = 2.4 RU / 1.8 μm , **Medium grid = 1.4 RU / 1.0 μm** , and Low grid = 0.7 RU / 0.6 μm .

Performing Bio-AFM on Live Cells

Live Cell Imaging and Manipulation with Nanosurf Bio-AFM

The study of biological systems ranges from whole organisms, organs and organoids down to their building blocks: cells and proteins. At the lower end of the length scale, atomic force microscope (AFM) systems have found their way into various disciplines of biological research, e.g. imaging of live cells and bacteria, single-cell manipulation, or force spectroscopy on molecules, cells or even tissue. In this application, advanced biological experiments on cells and how certain accessories can be used to perform them are discussed.

Keywords or phrases: Bio-AFM, Atomic Force Microscopy, FluidFM® technology, force spectroscopy, cell stiffness, manipulation.

Introduction

1. Combining Bio-AFM with optical microscopy

Bio-AFM becomes particularly powerful when combined with other techniques, in particular with optical microscopy. For that reason, Nanosurf offers stages for all common brands of inverted microscopes. These stages are mounted to the body of the microscope, allowing the AFM to be placed on top of the bio-sample, between the condenser and objective. There is also a special, long-range condenser for DIC and phase contrast. Epifluorescence, confocal or STED images.

2. Establishing physiological conditions

Mammalian cells are prominent samples for Bio-AFM experiments. These experiments are often conducted at room temperature and with a pH-stabilizing, CO₂-independent buffer. Whereas these non-physiological conditions might be pragmatic and useful to answer

Application Showcase

some scientific problems, they are clearly not optimal. They prevent long-term experiments (> 4 h), as cells visibly deteriorate. Moreover, the validity of some scientific inferences is in question even within short time frames.

It has been shown that buffer conditions affect ion channel conductance¹, molecule update², can inflict phototoxicity³ and change cell stiffness⁴, whereas the temperature affects, e.g., cell stiffness⁴ and adhesion measurements⁵. To allow for physiological conditions in an experiment, Nanosurf offers accessories like the AFM-compatible Live Cell Incubator that provide temperature, humidity and CO_2 control.

3. Controlling the temperature

The Petri dish holder accommodates plastic and glass bottom dishes up to 50 mm in diameter and 10 mm in height. It can be used in standalone applications as well as in combination with optical light microscopy. The holder is equipped with heating elements that together with the TEC controller allows controlling the temperature of the sample in a range from ambient to 60 °C. The temperature can be held constant within 0.1 °C. For many cells, ideal proliferation can be ensured when maintaining the temperature at a stable 37 °C.

For temperature-critical experiments, local heating via the Petri dish holder may not be sufficient, because a temperature gradient between the edge of the Petri dish and the center is difficult to prevent. To reduce temperature gradients in the Petri dish, a heating option that elevates the temperature around the complete optical microscope and AFM is available. If the AFM is placed in an acoustic enclosure, heating can be applied to its complete volume.

For long term experiments⁶, a local Petri dish heater and global acoustic enclosure heater were combined, with the global heating targeting 35 °C, just below the target temperature of the Petri dish heater. This combines small gradients with a short response time after mounting a new sample or cantilever.

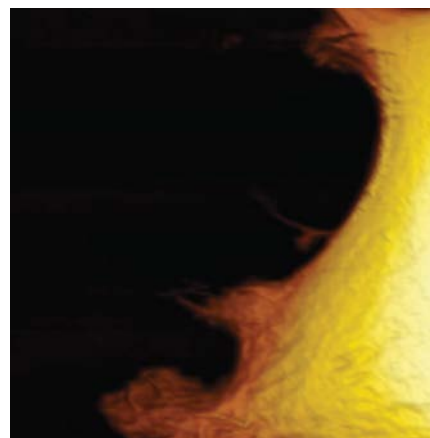
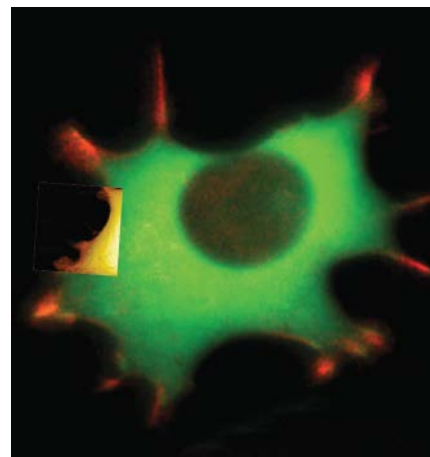


Figure 1: Live fibroblast imaged with inverted light microscope and AFM in cell culture conditions. Top, cell with genetically encoded fluorescent makers (actin-mcherry, gfp-paxillin). Bottom, AFM image, 10 μm width.

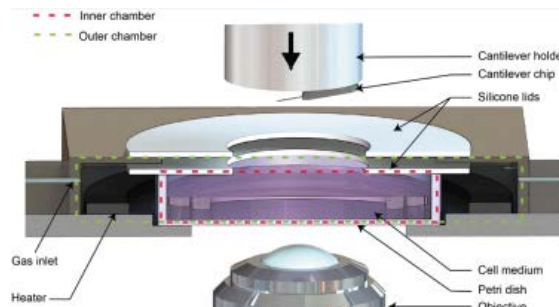


Figure 2: Schematic of the Live Cell Incubator.

Motorization of the AFM, optical microscope and stage mitigate the need to open the acoustic enclosure for laser alignment, finding areas of interest, or changing optical magnification or fluorescence filter set.

Application Showcase

The elevated temperature also increases the evaporation of the medium. To remedy this problem and, additionally, to control the pH of CO₂-dependent cell culture media, Nanosurf offers the Live Cell Incubator option.

4. Controlling humidity and pH

The Live Cell Incubator option is a modification to the standard Petri dish holder. It seals the Petri dish, creating two chambers, while still allowing to freely move the cantilever holder. The inner chamber is comprised of the closed Petri dish while the outer chamber encloses the Petri dish (Figure 2)⁷.

Combining the Live Cell Incubator with a suitable supply of humid gas, evaporation can be reduced to a minimum. The basic approach is to use a washing bottle to humidify bottled gas. In practice, this might be synthetic air with 5% CO₂, which allows to control the pH in CO₂-dependent cell culture media (e.g. DMEM).

Besides the basic humidification scheme, Nanosurf also offers an advanced humidification scheme. The advanced humidification scheme allows to control the humidity from ambient to 95% rel. hum. using a humidity sensor and microcontroller. If so desired, Nanosurf also offers a solution without the requirement for bottled gas, and the mixing of air with CO₂ is done in situ using line gas.

In the fashion described above, the experimental conditions can be kept the same as the cell culture. The correct temperature, low evaporation and pH-control not only ensure relevant insights into near physiological systems but also unlock experiments that unfold over the course of days, as for instance researching tissue formation⁶ with the PicoBalance.

5. Perfusion of cell media

While studying cells under physiological conditions is of great importance, research also requires disturbing the cells in a controlled fashion, e.g. by changing media. As an additional option to the Petri dish holder,

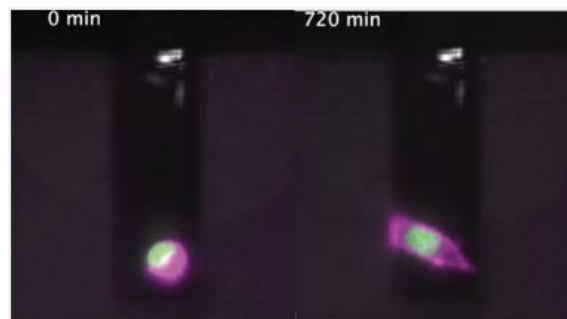


Figure 3: Identical cell at $t = 0$ and $t = 12$ h during cell mass measurement (PicoBalance) facilitated by the Live Cell Incubator.

Humidification schemes		
Basic	Advanced	Pro
Bottled gas, ≈90% rel. hum.	Bottled gas, ambient to 95% rel. hum.	Contr. gas mixing, ambient to 95% rel. hum.

Table 1: Humidification schemes overview.



Figure 4: Fluid inside the Petri dish can be added or removed using the perfusion insert.

Nanosurf offers the perfusion-insert (Figure 4). With the AFM on top of the Petri dish, ideally also enclosed by the Live Cell Incubator, exchanging media or adding chemicals to the Petri dish becomes more challenging. Particularly, if a certain area of the dish needs to be revisited, or if an experiment is to run autonomously, fluid-exchange or fluid insertion must be possible without human intervention. To allow for this, the perfusion insert consists of a ring, onto which two bent tubes are magnetically attached, which themselves are

Application Showcase

connected to flexible tubing. This tubing can then be connected to, e.g., syringes or pumps, which allows to add a fluid, or exchange media (push-pull-mechanism).

6. Single cell force spectroscopy

The 150 μm -stage is a Petri dish holder, which has long range piezo actuators integrated, allowing to precisely position and move the dish surface in height (z-axis) thus extending the z-range of the AFM. This is of particular interest in the field of single cell force spectroscopy (SCFS) but can also be used for 3D-printing and other applications. In SCFS, cell adhesion can be characterized down to the molecular level. For these experiments, cells can be attached to the cantilever via an adhesive protein and then brought in contact with the dish. After an optional waiting time, they are retracted. Even after the body of the cell is no longer in contact with the surface, adhesion events caused by tethers⁷ are recorded. A positioner for the microscope objective is also available.

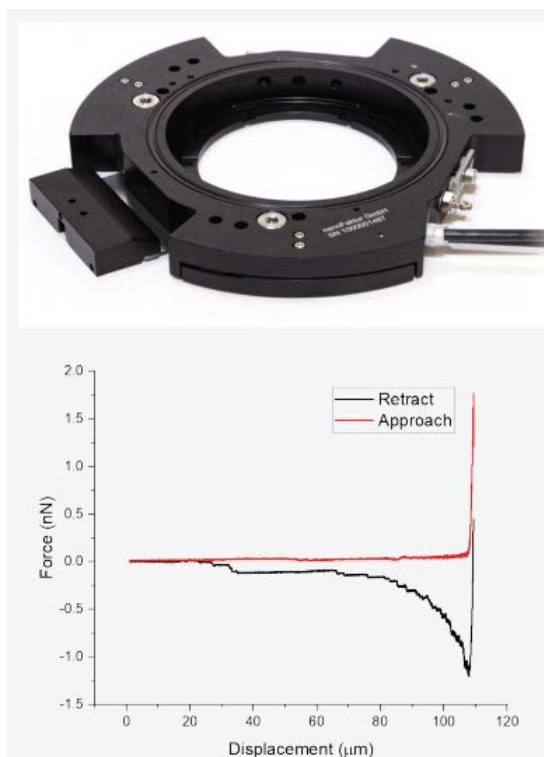


Figure 5: Petri dish holder with integrated piezo motors (top) enabling single cell force spectroscopy experiments (bottom).

7. Cell manipulation via FluidFM®

FluidFM combines the functionality of force-sensing cantilevers with that of micro-pipettes, offering a unique possibility of manipulating and probing cells. The FluidFM probe, which is a cantilever with an embedded microfluidic channel and aperture at the free end, allows to partially aspirate the cell, using under pressure. As the holding force between cantilever and cell is considerably higher than using adhesive proteins alone, the adhesion of fully adherent cells can be probed. It also allows for high throughput measurements of single cell adhesion⁹.

Using FluidFM probes that are micro-syringes instead of micropipettes extends FluidFM's functionality even further. These micro-syringes can be used for targeted micro-injection of cells or the reverse, the extraction of cell fluid¹⁰, e.g., for the purpose of TEM, protein assays and PCR or even single cell transcriptomics¹¹.

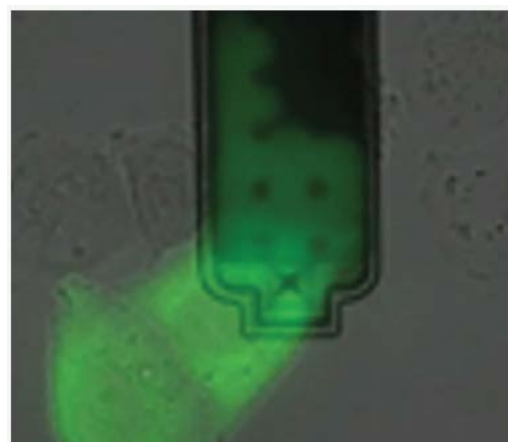


Figure 6: Extraction of sub-picolitre sample of nucleoplasm and cytoplasm from live cells without killing them.

Conclusion

Biological experiments often come with a set of specific requirements. These can relate to establishing a favourable, near-physiological environment in terms of temperature, humidity, and CO₂, or to manipulating the sample, in this case the cell, via the administration of chemicals, separating it from the dish surface. By providing this variety of accessories, in particular the different options for Petri dish holders (heater, Live Cell

Application Showcase

Incubator, perfusion-insert, and piezo-motors), Nanosurf hands researchers the tools to maximize the potential of AFM in biological applications.

List of mentioned accessories

The experiments outlined in this application note were performed with a DriveAFM on a Zeiss inverted optical microscope. Components and accessories used:

- » Petri dish holder with heating
- » Live Cell Incubator
- » Perfusion insert
- » 150- μ m piezo stage
- » FluidFM®

References

1. Hanrahan, J. W. & Tabcharani, J. A. Inhibition of an outwardly rectifying anion channel by HEPES and related buffers. *J. Membr. Biol.* 116, (1990).
2. Otero, D. et. al. Effects of 4-(2-hydroxyethyl)-1-piperazine-ethanesulfonic acid (AH5183) on rat cortical synaptosome choline uptake, acetylcholine storage and release. *Brain Res.* 359, (1985).
3. Lepe-Zuniga, J. L., Zigler, J. S., Jr & Gery, I. Toxicity of light-exposed Hepes media. *J Immunol. Methods* 103, (1987).
4. Chiou, Y-W. et. al. The Influence of Physical and Physiological Cues on Atomic Force Microscopy-Based Cell Stiffness Assessment. *PLOS One* 8, (2013).
5. Rico, F. et. al. Temperature Modulation of Integrin-Mediated Cell Adhesion. *Biophys J.* 99, (2010).
6. Martínez-Martín, D. et. al., Inertial picobalance reveals fast mass fluctuations in mammalian cells. *Nature* 550, (2017).
7. Martinez-Martin, D., Müller, D. J., Martin, S., Alsteens, D., Fläschner, G. WO2017012708A1, (2016).
8. Sun, M., Graham, J. S., Hegedus, B., Marga, F., Zhang, Y., Forgacs, G. and Grandbois, M., Multiple membrane tethers probed by atomic force microscopy, *Biophys. J.* 89, (2005).
9. Qiu, Y., et. al. Extending applications of AFM to fluidic AFM in single living cell studies. *J. Cell Physiol.* 237, (2022).
10. Guillaume-Gentil, O. et. al., Tunable Single-Cell Extraction for Molecular Analyses. *Cell* 116, (2016)
11. Chen, W. et. al., Live-seq enables temporal transcriptomic recording of single cells. *Nature* 608, (2022).



Bio-AFM

ODYSSEY M

THE UNMATCHED
VERSATILITY OF MULTIPLE
INSTRUMENTS IN ONE



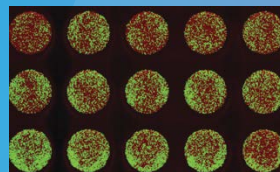
- DOZENS OF ASSAYS
- UP TO 19 CHANNELS
- 5- MICRON RESOLUTION
- MINUTES NOT HOURS



PROTEIN ARRAYS



IN - CELL WESTERN™ ASSAY



FLUORESCENT PROTEIN ASSAYS



FLUORESCENT WESTERN BLOT

Specifications	Details
Total Image Area	25 cm W x 18 cm D (9.8" W x 7.1" D)
Chemi Region Image Area	15 cm W x 11 cm D (5.9" W x 4.3" D)
Pixel Resolution	5, 10, 20, 50, or 100 μ m
Dynamic Range*	> 6 logs for chemiluminescence (optional) and fluorescence
Detectors	Sensor for chemiluminescence, sCMOS image sensor, CCD (pixel size 6.45 μ m)
Laser Lifetime	685 nm & 785 nm: 20,000 hours; 488 nm & 520 nm: 40,000 hours
Laser Classification	Class 1 laser product
Light Sources	RGB LED (trans-illumination), RGB LED (reflective illumination), Solid-state diode lasers: 488 nm, 520 nm, 685 nm, 785 nm
Focusing	Microscope adjustable -1.00 to 5.00 mm above scan bed

Bioluminescence (BLI) & Chemiluminescence Imaging using Irradiators

Preclinical Imaging and Radiation Therapy with Precision X-Ray SmART+ and X-Rad Systems

This application highlights potent preclinical research solutions provided by the combination of bioluminescence and chemiluminescence imaging with Precision X-Ray's SmART+ and X-Rad systems, enhanced by the OptiMAX module. In addition to supporting accurate radiation delivery and enabling real-time monitoring of tumour dynamics and therapy responses, these sophisticated multimodal imaging system improves detection sensitivity and resolution. Researchers can evaluate the effectiveness of new medication therapies, look into changes in the tumour microenvironment, and improve radiotherapy procedures by combining the SmART+ platform with OptiMAX. Preclinical irradiators are more accurate thanks to bioluminescence imaging's capacity to visualise both anatomical and molecular features, which eventually advances cancer research and treatment development.

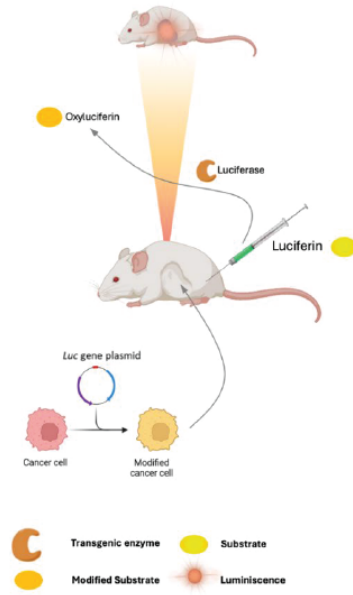
Keywords or phrases: Bioluminescence, chemiluminescence, preclinical imaging, radiation therapy, tumour microenvironment, image-guided radiotherapy, in vivo imaging, cancer, radiobiology, molecular imaging

Introduction

Bioluminescence and chemiluminescence are captivating phenomena involving the emission of light through biological processes and chemical reactions, respectively (Figure 1). Bioluminescence is the production and emission of light by living organisms, occurring through biochemical reactions involving luciferins (light-emitting molecules) and luciferases (enzymes that catalyze the reaction). Chemiluminescence refers to light emission resulting from a chemical reaction, occurring in both biological and non-biological contexts. Unlike bioluminescence, it is not exclusive to living organisms.

Application Showcase

BIOLUMINESCENCE



CHEMILUMINESCENCE

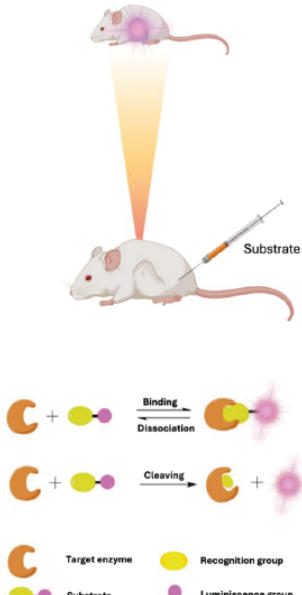


Figure 1: Overview of bioluminescence processes (left) and chemiluminescence processes (right).

The Precision X-Ray, Inc. SmART+ and X-Rad family are state-of-the-art preclinical irradiators, which can be enhanced with advanced imaging capabilities through the OptiMAX module, offering Optimized Detection, an Enhanced Imaging Workflow, and Advanced Software. The integration supports a wide range of applications, including Preclinical Imaging of Tumour Response to Radiation, Evaluating the Efficacy of Novel Drug Treatments, and Tumour Microenvironment and Therapeutic Responses, as described in examples below-

1. Radiotherapy-Induced Astrocyte Senescence Promotes an Immunosuppressive Microenvironment in Glioblastoma to Facilitate Tumour Regrowth

In this study¹, mice were cranially irradiated with a single-fraction dose of 10 Gy using the X-RAD225 OptiMAX (manufactured by Precision X-Ray) at 225 kV, 13.3 mA, 2.05 Gy/min with a 2-mm aluminium filter.

The device was equipped with a custom collimator to deliver a 20 mm-diameter iso-dose field while shielding the rest of the body. This irradiation setup was critical for inducing radiation-induced senescence in astrocytes, which were later found to promote an immunosuppressive tumour microenvironment facilitating glioblastoma regrowth. Thus, the SMART+ platform was a core component in enabling the study of radiation effects *in vivo*.

2. NRP1 inhibition modulates radiosensitivity of medulloblastoma by targeting cancer stem cells

Precision X-Ray was utilized to enhance the accuracy of radiation therapy in medulloblastoma (MB) models². By combining precise radiation delivery with the inhibition of Neuropilin-1 (NRP1) using the peptidomimetic agent MR438, the researchers were able to selectively target tumour cells while minimizing damage to surrounding healthy tissue. This precise modulation of radiation

Application Showcase

allowed for improved tumour control and a significant reduction in cancer stem cells, providing a promising strategy for reducing radiation doses while enhancing therapeutic efficacy in MB treatment.

3. Imaging Performance of a Multimodal Module to Enhance Preclinical Irradiator Capabilities

Precision X-Ray's OptiMAX imaging system was integrated into a preclinical irradiator to enhance imaging capabilities for both X-ray and bioluminescence applications³. The system, which uses a cooled CCD camera and a phosphor screen, allows for high-resolution imaging by capturing radiographic and optical images with a single sensor. The X-ray images demonstrated excellent spatial resolution (2.5-line pairs per millimetre) and high contrast sensitivity, while bioluminescence imaging provided detailed insights into the activity of cancer cells *in vivo*. This multimodal imaging approach improves the preclinical irradiator's ability to conduct image-guided radiotherapy, offering better anatomical and molecular visualization, essential for optimizing radiotherapy protocols in animal models.

Conclusion

The integration of Bio/Chemiluminescence Imaging (BLI) with the Precision Smart+ and XRAD systems, enhanced by OptiMAX, marks a significant improvement in the imaging capabilities of these systems. This integration facilitates targeted radiation delivery and allows for effective monitoring of processes and their efficiency. Additionally, these imaging capabilities can be employed independently of radiation for research purposes. This combination enhances preclinical research. sensitivity, resolution, and workflow efficiency, facilitating a broad spectrum of applications in preclinical research.

References

1. Ji, J., Ding, K., Cheng, B., Zhang, X., Luo, T., Huang, B., & Chen, G. (2024). Radiotherapy-Induced Astrocyte Senescence Promotes an Immunosuppressive Microenvironment in Glioblastoma to Facilitate
2. Douyère, M., Gong, C., Richard, M., Pellegrini-Moïse, N., Daouk, J., Pierson, J., ... & Boura, C. (2022). NRP1 inhibition modulates radiosensitivity of medulloblastoma by targeting cancer stem cells. *Cancer Cell International*, 22(1), 377.
3. Daouk, J., Jubréaux, J., Chateau, A., Schohn, H., & Pinel, S. (2020). Imaging performance of a multimodal module to enhance preclinical irradiator capabilities. *Clinical Oncology and Research*, 3(2).

Tumor Regrowth. *Advanced Science*, 11(15), 2304609.

2. Douyère, M., Gong, C., Richard, M., Pellegrini-Moïse, N., Daouk, J., Pierson, J., ... & Boura, C. (2022). NRP1 inhibition modulates radiosensitivity of medulloblastoma by targeting cancer stem cells. *Cancer Cell International*, 22(1), 377.

3. Daouk, J., Jubréaux, J., Chateau, A., Schohn, H., & Pinel, S. (2020). Imaging performance of a multimodal module to enhance preclinical irradiator capabilities. *Clinical Oncology and Research*, 3(2).

PRECISION
X-RAY IRRADIATION



X-RAY SmART+

CyteFinder II HT Instrument

Immunofluorescence Imaging for Rare Cell Detection

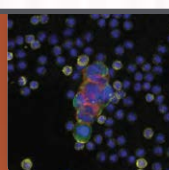
CyteFinder II Instruments are high-speed, whole slide imaging systems with options for multiplexed liquid biopsy and tissue spatial analysis.

Advantages

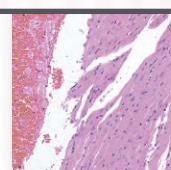
- ◆ CyteFinder II HT is designed to meet the demands of high-volume pathology labs.
- ◆ Offers hands-free, rapid whole slide scanning of up to 80 slides.
- ◆ Features a barcode-driven workflow for efficient sample tracking.
- ◆ Utilizes machine learning for:
 - ◆ Rare cell detection
 - ◆ Automated tissue finding
- ◆ Ideal for clinical researchers conducting:
 - ◆ Cellular or
 - ◆ Tissue-based multiplexed analysis.



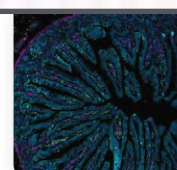
RARECYTE
Precision Biology for Life Sciences



CTC cluster from
breast cancer patient



H&E imaging of mouse
heart tissue



High resolution, multiplexed
tissue imaging

Detection of Adulterants in Morphine Sulphate Solutions

A Portable and Precise Method Using UV/Vis NanoPhotometer® Instrumentation

Katherine A. Roberts, PhD¹ and Thomas Sahiri, PhD²

¹ California State University, Los Angeles; ² President, Implen, Inc. Westlake Village, CA

A growing problem among California's Emergency Medical Services is the theft of morphine from vials that are stored in their emergency vehicles and substituting the morphine with saline or other solutions. This application focuses on this specific problem. The objective was to develop and test a simple, rapid, reliable and reproducible procedure to detect whether a morphine sulphate solution has been adulterated.

The research was restricted to diluting a 4 mg/ml dose of morphine sulphate contained in a carpuject cartridge. The following four solutions were used to dilute morphine sulphate: nanopure water, saline, diphenylamine, and epinephrine. The effect of diluting morphine sulphate with

each of the solutions was measured by UV/VIS spectrophotometry using an Implen NanoPhotometer®.

Ten replicate measurements of the absorbance values were obtained for five concentrations of each adulterated morphine solution to determine the mean absorbance values.

Keywords or phrases: UV/Vis spectrophotometry, absorbance, morphine, NanoPhotometer

Introduction

The literature on the subject of drug tampering activity (scholarly or otherwise) is limited to a few articles, a book and a number of newspaper reports. The limited literature concerns the restricted areas where the

Application Showcase

tampering activity takes place. In hospitals, access to controlled substances is secured and available only to authorized professionals, some of whom take advantage of their privileges to tamper with drugs away from peer oversight and public scrutiny.

The tampering of drugs aboard a medical emergency vehicle is even more difficult to detect. The vehicles are constructed to block public view from the interior area where patients are treated and transported. Thus, only two operators have immediate and continual access to morphine and potential drug diluents.

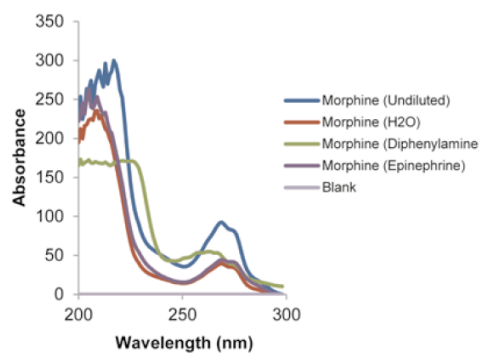
These individuals often form a close camaraderie and become bound by a mutual code of silence in an environment that is highly conducive to tampering. An overwhelming number of tampering cases go undetected, unreported and unexamined, with press accounts surfacing only when they bear serious consequences.

Purpose of Study

The study was designed to create a rapid, reproducible, reliable, robust and ostensibly cost-effective analytical approach to detect cases of tampered morphine.

A NanoPhotometer® instrument (Implen, Inc.) was evaluated to determine if it meets these criteria.

Morphine Dilution Series (2 mg/ml)



Results

The analysis focused on adulterating morphine sulphate solutions with various substances/pharmaceuticals commonly available to emergency medical technicians. Serial dilutions of morphine sulphate were also prepared with each adulterant to simulate tampering.

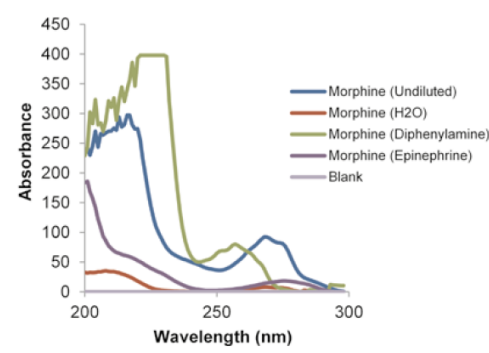
A UV/VIS NanoPhotometer® instrument was evaluated as a potentially viable technique to detect the presence of an adulterant in morphine sulphate.

Materials and Methods

The pharmaceuticals were supplied to CSULA by the Ventura County Emergency Medical Service Agency in conjunction with the County Pharmacy Administration of Los Angeles. The following materials were utilised:

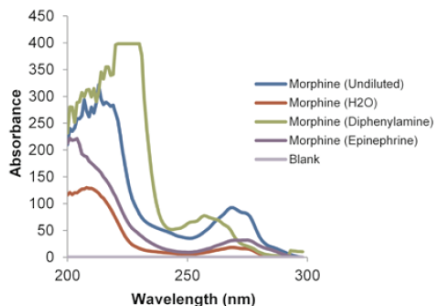
4 mg/ml morphine sulphate and 0.9% Sodium Chloride Injection (Hospira); 50 mg/ml diphenhydramine (Baxter Healthcare); 2.5 mg/ml epinephrine (manufacturer unknown). In addition, physiological saline (0.9%) and nanopure water were used as diluents. A 2 µL sample volume was used for each analysis and all samples were analysed in replicates of 10.

Morphine Dilution Series (0.25 mg/ml)

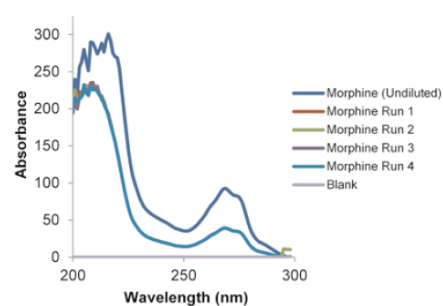


Application Showcase

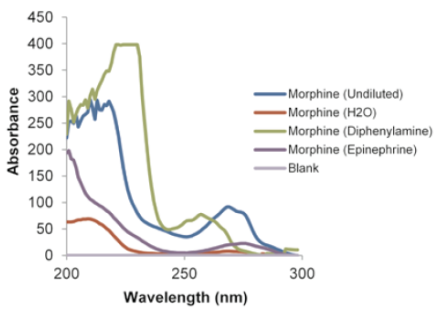
Morphine Dilution Series (1 mg/ml)



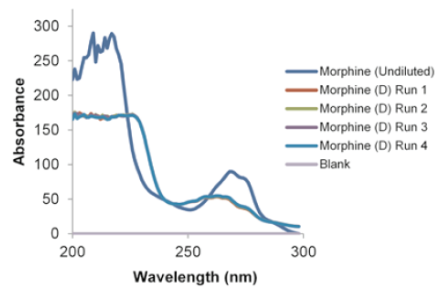
Morphine H₂O Dilutions (2 mg/ml)



Morphine Dilution Series (0.5 mg/ml)



Morphine Diphenylamine Dilutions (2 mg/ml)



Conclusion

With respect to the adulterants evaluated, the findings support that the Implen NanoPhotometer® instrument provides an affordable, sensitive, reliable and portable screening test to detect tampered morphine.

Adulterated morphine was detected based on either qualitative (diphenylamine) or quantitative (saline, nanopure water, and epinephrine) differences observed in the UV spectra.

A linear relationship was established between the mean morphine concentration of morphine and the corresponding absorbance, in accordance with Beer's law. It was determined that the saline, nanopure water and epinephrine adulterants did not interfere with absorbance of morphine at 269 nm, as observed by the linear

refractometers to detect controlled-substance tampering. American Journal of Hospital Pharmacists, 48, 1488-92

Gill D, Goodwin S, Knudsen A, & Wade C. (1990). Refractometer screening of controlled substances in an operating room satellite pharmacy. American Journal of Hospital Pharmacists, 47, 817-18.

O'Neal B, Bass K, & Siegel J. (2007). Prevention of controlled substance diversion—scope, strategy, and tactics. Hospital Pharmacy, 42, 359-67.



NanoPhotometer®
NP80



Select References

Cheung J, Chong S, Kitrenos J, & Fung H. (1991). Use of



dPette+

Multi-functional 8-channel Electronic Pipette

High-performance 8-channel electronic pipette with intuitive use and ergonomic design for efficient, reproducible sample transfers.



• Easy Operation

Intuitive interface for setting functions and parameters.

• Convenient and Versatile

360° pipetting. Double knobs for simple and versatile control. Easy loading tip cones offers smooth and leak free operation.

• Ergonomic Design

Low operation forces for complete work, which is exceptionally fatigue-free.

• Dual charging modes

Use of USB charger or the charging stand to ensure uninterrupted use.

Developing a 3-Color Western Blot

A 3-color Western blot has the benefits of saving time, reducing sample usage and improving data quality. However, there is complication involved. Every stage necessitates meticulous preparation and optimisation, from choosing the appropriate antibodies and blocking buffers to guaranteeing spectral compatibility and operating within a common linear range.

This guide breaks down the key considerations and best practices to help design and execute your 3-color Western blot experiments.



The popularity and longevity of Western blotting are due to how much information can be obtained from a properly controlled and executed experiment. Western blotting uses specific antibodies to detect a target protein in a complex protein mixture that has been immobilized on a membrane.

Western blotting can provide information about target protein size, relative target abundance, target location (if the sample was fractionated), and if the target is affected by a treatment (e.g., drug, small molecules, temperature shift).

Over time, the desire to detect multiple proteins within a sample has emerged, leading scientists to develop several methods for simultaneous protein detection on a single membrane—including multiplexed Western blots. Western blot data is only as good as the antibodies used and the attention given to the parameters of the experiment. This is especially true when trying to perform a spectrally distinct 3-color Western blot. The parameters include but may not be limited to:

- » Membrane type
- » Gel type
- » Transfer conditions
- » Blocking buffer selection
- » Primary/secondary antibody compatibility (especially with host derivation and target species)
- » Combined antibody linear range

I. Determine Your Targets and Sample Type

First, determine what target proteins you would like to detect, then determine if all of your targets are expressed in a single sample. If all your targets are not expressed in your sample, you may be able to find an alternative sample type,

such as a transfected lysate or knock-in cell line, that may work depending on your experimental needs.

There are several different ways to determine if all of your targets are expressed in a single sample.

- » Start with your lab
- » Search citations
- » Check manufacturer and vendor websites
- » Explore GeneCards®

GeneCards®: The Human Genome Database catalogues the expression of genes in human tissue and orthologs of that gene in animals—including animals that do not express that gene.

II. Know Your Molecular Weights

The molecular weight is important when determining the correct gel percentage and type for SDS-PAGE. These factors will help you choose the right transfer conditions and attain the best resolution of bands.

Large proteins generally require a lower percentage acrylamide and transfer better with low methanol and extended transfer times.

Small proteins require a high percentage acrylamide, high methanol concentrations, and shorter transfer times to bind them to the membrane and keep them from passing through the membrane.

III. Determine the Right Membrane

If your lab is already using one or two antibodies, identify what membrane was used for your antigen-antibody pairs. The chemistry of PVDF and nitrocellulose membranes differ, which makes them unique in their protein binding, chemical resistance, and background noise.

If your antibody-antigen pairs have not been tested on both, it is worth the time to determine which membrane gives you the best signal-to-noise ratio.

IV. Choose the Right Blocking Buffer

Blocking buffer is crucial when using multiple antibodies. No single blocking buffer will be optimal for every antigen-antibody pair. Some primary antibodies are dramatically affected by blocking conditions.

Look for a blocking buffer that provides:

- » Strong signals for the expected band(s)
- » Low membrane background
- » Ideally, no non-specific background bands from the primary antibody

Try at least three different types of blocking buffer to determine which gives you the best signal with the lowest background for each target by themselves.

V. Select Your Antibodies Carefully

Your choice of antibodies is critical for a 3-color Western blot.

Antibody selection can be challenging.

- » Visible fluorescent secondary antibodies should be used for your target with the highest abundance to minimize the background inherent at these wavelengths.
- » Near-infrared fluorescent secondary antibodies should be used for proteins with lower abundance. All targets must be detected within the same linear range.

Verify Primary Antibodies

If you have existing information for one or two target antibodies, verify:

- i. That the antibody has been used for detection of your target in your chosen sample type.
- » If it has, confirm the correct primary antibody concentration in your own experiment to establish the linear range.
Use the same blocking buffer as was used before
- » If not, try the vendor's suggested dilution. If you are given a dilution range, first try the middle of that range. Detect your target in a dilution series of your sample type using a minimum of three different blocking buffers. Choose the most suitable blocking buffer, then determine the antibody concentration that provides the best signal-to-noise ratio.

- ii. The linear range using the optimum antibody concentration and blocking buffer using a dilution series of your sample.

Keep Host Species in Mind

Your primary antibodies must be derived from different host species, so they can be distinguished by secondary antibodies of different specificities.

Your secondary antibody source must match your primary antibody host species.

Antibodies generated in species that are closely related—such as mouse and rat or goat and sheep—should not be multiplexed together. This is because the secondary antibodies will cross-react with both species.

To help with pairing antibodies, take advantage of the specificity of different mouse monoclonal IgG subclasses (e.g., IgG1, IgG2a, IgG2b). Then, you can use IRDye® subclass specific secondary antibodies for multiplex detection. Be sure to confirm the specificity of the subclass when using this type of pairing.

Example Screening of Multiple Antibodies

Eight antibodies were screened at once using the MPX™ Multiplexer Blotting System. The antibodies were screened with two separate blocking buffers and five secondary antibodies. The antibodies used for screening include a whole antibody goat anti-mouse (GaM) secondary as a positive control, three different mouse subclass antibodies, a rabbit primary, and a goat primary. The use of two blocking buffers provided the bonus of establishing a blocking buffer for the antibodies.

If the antibodies were not already optimized in the lab, they were diluted using vendor recommendations. The same was true for the secondary antibodies. The nitrocellulose membrane had already been optimized in past experiments.

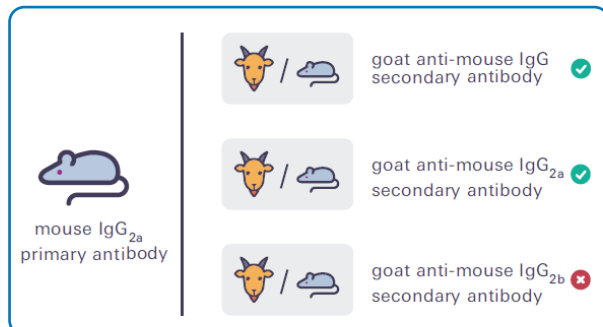
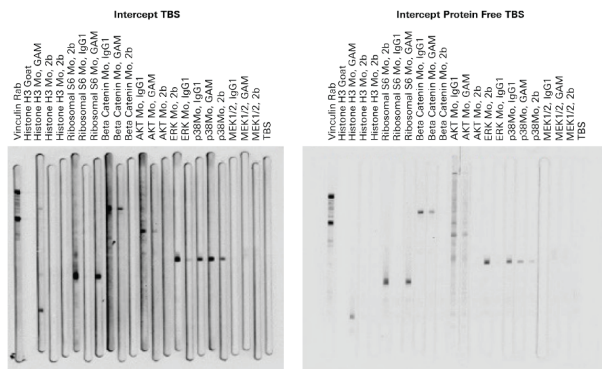


Figure 1. Your secondary antibody source must match your primary antibody host species. For primary antibodies of the same host species but different IgG subclasses, ensure you are using a subclass-specific secondary antibody. For example, when using a mouse IgG_{2a} primary antibody, use a goat anti-mouse IgG or IgG_{2a} secondary antibody but not a goat anti-mouse IgG_{2b} secondary antibody.



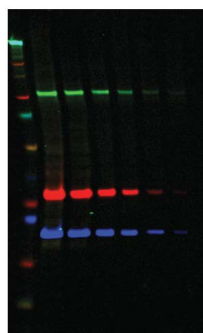
Target	Host Species	Isotype	Primary Antibody			Secondary Antibody		
			Mouse IgG	Mouse IgG1	Mouse IgG2b	Rabbit IgG	Goat IgG	
Vinculin	Rabbit	IgG				✓		
Histone H3	Goat	IgG					✓	
Histone H3	Mouse	IgG	✓					
Ribosomal S6	Mouse	IgG2b	✓		✓			
Beta Catenin	Mouse	IgG1	✓	✓				
Akt	Mouse	IgG1	✓	✓				
ERK	Mouse	IgG2b	✓		✓			
p38	Mouse	IgG1	✓	✓	✗			
MEK1/2	Mouse	IgG1						
Intercept® (TBS) Blocking Buffer only								

Table 1. Individual antibody detection using subclass specific secondary antibodies. A ✓ indicates a positive result with the secondary antibody. All mouse subclass antibodies react with the goat anti-mouse whole IgG secondary as expected, except for MEK 1/2. The primary antibody was run in the gel. In the MPX™ System image, Mo = mouse, Rab = rabbit, and GAM = goat anti-mouse.

The results in Table 1 indicate the expected reactivity, with the exception of anti-p38 and anti-MEK 1/2. Anti-p38 showed cross-reactivity with IgG_{2b} secondary antibody. Anti-MEK 1/2 was not recognized by any secondary antibody in either blocking buffer.

Example of Successful Antibody Combination

A Western blot using a two-fold serial dilution of NIH3T3 lysate starting at 20 µg per lane. The subclass specificity of the mouse monoclonals was exploited so that two mouse primary antibodies and one rabbit primary antibody could be combined and detected using two goat anti-mouse subclass specific secondary antibodies and a goat anti-rabbit secondary antibody.



Target	Primary Antibody	Secondary Antibody	Color
Beta Catenin	Mouse IgG1	IRDye® 800CW Goat anti-Mouse IgG1	Green
Ribosomal S6	Mouse IgG2b	IRDye® 680LT Goat anti-Mouse IgG2b	Red
Cofilin	Rabbit	VRDye™ 549 Goat anti-Rabbit	Blue

Examples of Problematic Antibody Combinations

1. Rat and mouse antibody combinations are not recommended unless experiments have been performed to confirm that the secondary antibodies, goat anti-mouse and goat antirat, do not cross-react. This is regardless of the secondary host, goat, or donkey combinations.

Target	Primary Antibody	Secondary Antibody
X	Mouse	IRDye® 680RD Goat anti-Mouse
Y	Rabbit	VRDye™ 549 Goat anti-Rabbit
Z	Rat	IRDye 680RD Goat anti-Rat

2. In this case, either the goat primary or a different host other than goat conjugated secondary antibody would need to be selected in order for this 3-color Western blot to work.

Target	Primary Antibody	Secondary Antibody
X	Mouse	VRDye 549 Donkey anti-Goat
Y	Goat	VRDye™549 Goat anti-Rabbit
Z	Human	IRDye 680RD Goat anti-Human

VI. Find the Combined Linear Range

You will want to find the combined linear range for all antigen-antibody combinations. Why is this important?

The linear range is the range of sample loading that produces a linear relationship between the amount of target on the membrane and the signal intensity recorded by the detector.

If signal is linear, doubling the protein concentration should lead to an approximate doubling of the signal intensity. Outside this range, signal intensity is not dependent on sample loading and does not accurately reflect the amount of target present which means quantification is not accurate.

Graphing the signal vs. sample loading of your target and then establishing the linear range allows quantification to be accurate. Quantitative Western blot analysis is accurate only if the target proteins and internal loading control can be detected within the same linear range. As a result, you must work within the combined linear range of all the antibodies in your multiplexed experiment.

Examples of Combined Linear Range with Multiple Targets

Due to the number of antibodies used, 3-color Western blots will generally have a narrow combined linear range.

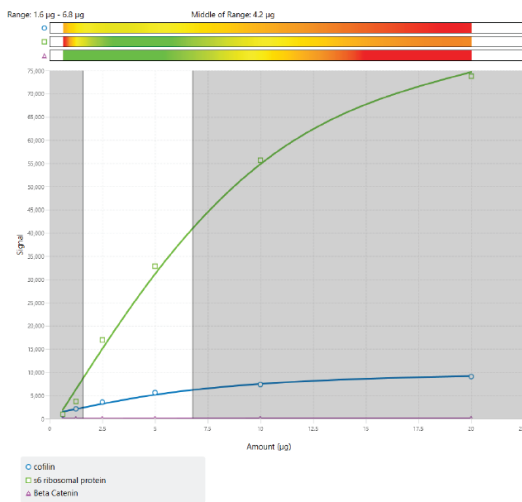


Figure 2: An example using Empiria Studio® Software to determine the combined linear range of rabbit anti-cofilin, mouse IgG2b anti-S6 ribosomal protein, and mouse IgG1 anti-beta-catenin primary antibodies in a two-fold serial dilution (20 to 0.625 μg) of NIH3T3 cell lysate. In this Western blot, the combined linear range is 1.6 μg to 6.8 μg, with the midpoint of the range at 4.2 μg.

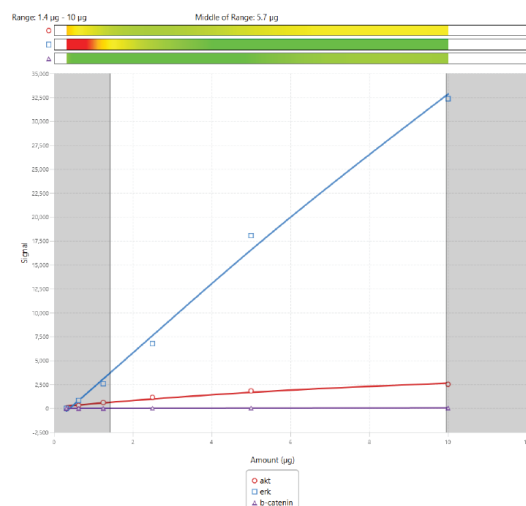


Figure 3: An example using Empiria Studio® Software to determine the combined linear range of mouse IgG1 anti-beta-catenin, rabbit anti-AKT, and mouse IgG2b anti-ERK primary antibodies in a two-fold serial dilution (10 to 0.625 μg) of NIH3T3 cell lysate. In this Western blot, the combined linear range is 1.4 μg to 10 μg, with the midpoint of the range at 5.7 μg. This combination of antibodies provides a relatively wide combined linear range.

VII. Conclusion

The wide variety of visual secondary antibodies offers seemingly endless possibilities for target protein detection. However, visual dyes can be tricky to work with and may require much more planning for multiplexed experiments. For Western blots, the higher background of visible wavelengths will be an ongoing issue, as will pairing three antibodies in a single experiment that can all be detected within a combined linear range. Pairing two antibodies with a total protein stain, such as Revert™ 520 Total Protein Stain, is a robust alternative for those who plan to normalize. Either option (three antibodies or two antibodies with a total protein stain) is substantially better than stripping and re-probing membranes. With proper research, careful planning, and a moderate amount of optimization, you can produce solid, successful, and quantitative 3-color Western blots.

C-DiGit® Blot Scanner

Discover more with better technology.



 LICORbio™

Product Highlight

LightIR™

FLEXIBLE IN VIVO NIR FLUORESCENCE IMAGER

The LightIR™ is a cutting-edge in vivo fluorescence imager that delivers exceptional sensitivity and versatile functionality, seamlessly integrating open-environment operation and light-tight enclosure capabilities into a single instrument.

Flexibility

- › The LightIR™ can be used for fluorescence guided surgery, on small and large animals using either the closed setup or the optical head open configuration
- › NIR-I and NIR-II fluorescence versions are available

Sensitivity

- › The laser excitation combined to a patented real-time background subtraction and brightfield overlay makes it a highly sensitive system, adapted to various light environments
- › For NIR-II, coupled to the Alizé 1.7, a high-end scientific-grade InGaAs camera, it offers low noise levels, high efficiency, and a rapid frame rate

Technical Specifications

Imaging modes	NIR-I or NIR-II Fluorescence, brightfield, subtracted, overlay Optional: RGB brightfield
Real-time processing	background subtraction, brightfield/fluorescence overlay
Emission spectral range	NIR-I: 650 - 900 nm NIR-II: 900 - 1600 nm
Fluorescent channels	1 or 2 channels
Available excitation wavelengths	640 nm, 690 nm, 750 nm, 785 nm, 808 nm, 980 nm
Emission filters	set according to chosen excitation wavelengths
Field of view	7 cm x 7 cm
Detector	CMOS (NIR-I) or Alizé 1.7 InGaAs (NIR-II)
Image size (px)	1024 x 1024 (NIR-I) or 512 x 512 (NIR-II)
Output format	tiff images (16 bits) with metadata



Advantages

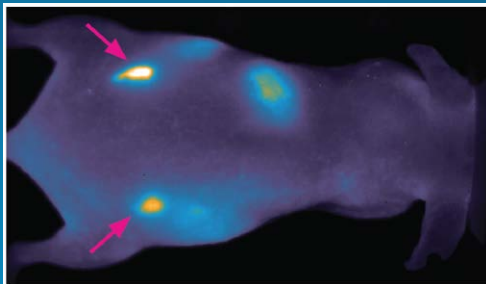
- › High sensitivity due to high power excitation and background subtraction
- › Real time image display
- › User friendliness
- › Acquisition sequence programming
- › Preclinical Surgical Ready
- › Flexible for an open environment operation and light-tight enclosure

Product Highlight

Applications

- › Fluorescent guided surgery
- › Fluorescent agent biodistribution
- › Deep tissue lymphatic imaging
- › Vascularisation imaging
- › Infectious diseases studies

Cancer Imaging



Lymphatics imaging in mouse with ProimagingCJ215 and NIR-II fluorescence



Tumor labeling with Fluoptics' AngioStamp™, targeting integrin expression

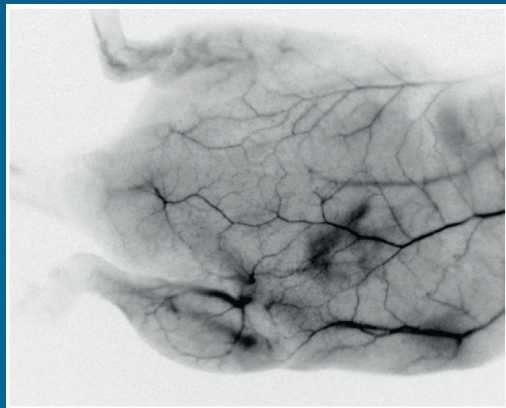
Courtesy V. Josserand, Optimal, Grenoble, France

Lymphatics



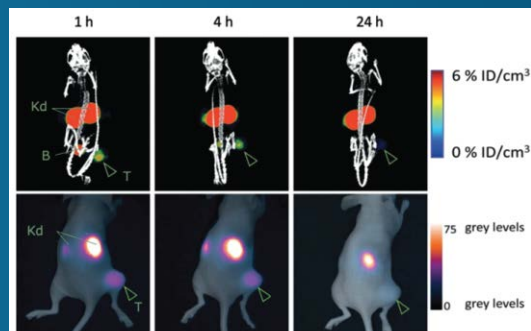
Lymphatics imaging in mouse with ProimagingCJ215 and NIR-II fluorescence

Vascular Imaging



Vascular imaging in mouse with NIR-II fluorescence.
Courtesy Optimal Imaging Platform, Grenoble, France

Fluorescence Guided Surgery



Anti HER2 Nanobodies conjugated with Cy5 and 111In-labeling of DTPA, SKOV3 murine models

Debie P et al. The Design and Preclinical Evaluation of a Single-Label Bimodal Nanobody Tracer for Image-Guided Surgery. *Biomolecules*. 2021 Feb 26

Compact system for NIR-I or NIR-II imaging on small and large animals

BENCHTOP HIGH SPEED REFRIGERATED CENTRIFUGE

M500TR

- Table Top Refrigerated Centrifuge, from microtubes to 500mL bottles, or micro-plates
- Ideal for general purpose centrifuge
- A newly developed 5-in-1 rotor. This one rotor is sufficient for use with various microtubes.

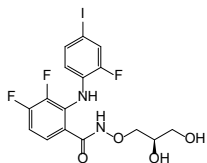
SPECIFICATIONS

Max. Speed	15,300 rpm
Max. RCF	22,250 xg
Max. Capacity	2,000 ml
Temperature Setting	-10 to +40°C



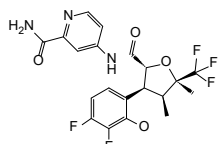


Recent novel FDA approved drugs



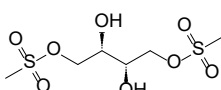
Mirdametinib

A kinase inhibitor, mirdametinib (Gomekli) treats neurofibromatosis type 1 in adults and paediatric patients who have symptomatic plexiform neurofibromas not cooperative to complete resection.



Suzetrigine

Suzetrigine (Journavx), a non-opioid, small molecule analgesic, that treats severe acute pain. It is a sodium channel blocker that targets a pain signalling pathway in the peripheral nervous system.



Treosulfan

Treosulfan (Grafapex) an alkylating drug is indicated in combination with fludarabine as a preparative routine for allogeneic hematopoietic stem cell transplantation in adult and pediatric patients >1 year old with Acute Myeloid Leukemia or Myelodysplastic Syndrome

Datopotamab deruxtecan (Datroway), an antibody drug conjugate made up of a monoclonal antibody and a topoisomerase inhibitor, used for the treatment of metastatic HR-positive, HER2-negative breast cancer and nonsquamous non-small cell lung cancer (NSCLC), in patients who have received prior systemic chemotherapy.

Industry Buzz



Pharmaceutical &
Lab Exhibition
Verna, Goa
May 2025



IPAAF International
Poultry, Aquaculture &
Animal Feed Expo,
Ernakulam, Kerala
May 2025



analytica Lab India
Analytica Lab India, Mumbai
April 2025

A sneak-peak at our events

CATALYST Cue invites scientists and industry specialists to share their expertise through articles on emerging scientific breakthroughs and instrumentation.



Please write to us at **info@inkarp.co.in**

CATALYST Cue is now available in digital format.



***Scan the QR Code
to leave your valuable feedback***

For latest news, insights, and discussions in the world of science, follow us on

Disclaimer: CATALYSTCue provides a platform for diverse perspectives. The views and opinions expressed in the articles and interviews are solely those of the authors.

Hei-SHAKE Orbital Core

The Hei-SHAKE Orbital Core has all the core functions required for the realization of any shaking application in the laboratory.

The all-rounder up to 15 kg



inkarp®
Your Knowledge... Our Solution...!

Authorised India Partner

Inkarp Instruments Pvt Ltd

Plot No - 5A/10-11, 3rd Floor, IDA Nacharam Road No. 1, Nacharam - Chilka Nagar Road, Hyderabad – 500076

📞 040 27172293/5088 📩 info@inkarp.co.in

18th - 20th September 2025, Hitex Hyd
Booth No: C21, Hall No: 03

 **analytica Lab India**